Award Number: W81XWH-11-1-0814

TITLE: Development of Technologies for Early Detection and Stratification of Breast Cancer

PRINCIPAL INVESTIGATOR: David R. Walt

CONTRACTING ORGANIZATION: Tufts University
Medford, MA 02155

REPORT DATE: October 2013

TYPE OF REPORT: Annual

PREPARED FOR: U.S. Army Medical Research and Materiel Command
Fort Detrick, Maryland 21702-5012

DISTRIBUTION STATEMENT: Approved for Public Release;
Distribution Unlimited

REPORT DOCUMENTATION PAGE

Form Approved
OMB No. 0704-0188

1. REPORT DATE	2. REPORT TYPE	3. DATES COVERED
October 2013	Annual	29 September 2012-28 September 2013

4. TITLE AND SUBTITLE

Development of Technologies for Early Detection and Stratification of Breast Cancer

5a. CONTRACT NUMBER

5b. GRANT NUMBER
W81XWH-11-1-0814

5c. PROGRAM ELEMENT NUMBER

6. AUTHOR(S)
Prof. David Walt: David.Walt@tufts.edu
Prof. Daniel Chiu: chiu@chem.washington.edu
Prof. Charlotte Kuperwasser: charlotte.kuperwasser@tufts.edu
Prof. Gail Sonenshein: gail.sonenshein@tufts.edu
Prof. Rachel Buchsbaum: rbuchsbaum@tuftsmedicalcenter.org

5d. PROJECT NUMBER

5e. TASK NUMBER

5f. WORK UNIT NUMBER

7. PERFORMING ORGANIZATION NAME(S) AND ADDRESS(ES)

Tufts University
62 Talbot Avenue
Medford, MA 02155

Tufts University School of Medicine
136 Harrison Avenue
Boston, MA 02111

University of Washington
4333 Brooklyn Ave NE
Seattle, WA 98195

Tufts Medical Center
800 Washington Street
Boston, MA 02111

8. PERFORMING ORGANIZATION REPORT NUMBER

9. SPONSORING / MONITORING AGENCY NAME(S) AND ADDRESS(ES)
U.S. Army Medical Research and Materiel Command
Fort Detrick, Maryland 21702-5012

10. SPONSOR/MONITOR'S ACRONYM(S)

11. SPONSOR/MONITOR'S REPORT NUMBER(S)

12. DISTRIBUTION / AVAILABILITY STATEMENT
Approved for Public Release; Distribution Unlimited

13. SUPPLEMENTARY NOTES

14. ABSTRACT

The overall goal of this work is to develop ultra-sensitive detection techniques to identify a panel of new biomarkers and indicators with diagnostic and predictive value in breast cancer. During year 1, we identified candidate breast cancer biomarkers and developed ultra-sensitive assays for several of them. Two different miRNA single molecule assay approaches have also been investigated and both showed promise for achieving similar ultrasensitive data using miRNA as targets. Continuing work on this assay includes increasing efficiency and decreasing the background. Circulating tumor cell isolation using microfluidics has been accomplished and these methods will soon be integrated with the single molecule detection approach. Good progress on identifying additional markers (miRNA, mtDNA, ADAM8) has been made. Further work to validate whether these markers are useful for detecting early stage breast cancer or tumor aggressiveness is underway. Finally, we have begun testing serum collected from a Human-in-Mouse (HIM) model of breast cancer using the assays developed.

15. SUBJECT TERMS

Single molecule detection, cancer biomarkers, ultra-sensitive protein assays, single cells, human-in-mouse model, miRNA, circulating tumor cells

16. SECURITY CLASSIFICATION OF:			**17. LIMITATION OF ABSTRACT**	**18. NUMBER OF PAGES**	**19a. NAME OF RESPONSIBLE PERSON**
					USAMRMC
a. REPORT	**b. ABSTRACT**	**c. THIS PAGE**		40	**19b. TELEPHONE NUMBER** *(include area code)*
U	U	U	UU		

Table of Contents

Page

The overall goal of this work is to develop ultra-sensitive detection techniques in order to identify a panel of new biomarkers and indicators with diagnostic and predictive value in breast cancer. During years 1 and 2 we will develop ultra-sensitive detection techniques and apply them to identifying prospective biomarkers using the Human-in-Mouse (HIM) model of breast cancer. During years 3-5 we will extend the findings in the HIM model to validate prospective biomarkers in human subjects with breast cancer. This work is broken down into specific tasks by investigator as follows:

INTRODUCTION

Despite the recent advances made in breast cancer diagnostics and treatment, it has been estimated that in 2012 the United States will diagnose approximately 200,000 new cases of breast cancer, resulting in approximately 40,000 deaths.[1] Mammography is a powerful imaging technique for tumor detection; however, it lacks the ability to decipher benign from cancerous tumors, is unable to detect tumors smaller than 1mm,[2] misses approximately 20% of breast cancers potentially present at the time of screening, and has an 8-10% false positive rate.[3] These drawbacks lead to inaccurate patient diagnosis, which can allow potentially fatal disease progression, or in the cases of over-treatment, unnecessary physical and emotional trauma.[4] ELISA, the most common immunoassay for measuring proteins from breast tumors, excised samples, and serum, has a lower detection limit of ~1-10 pM,[5] which is not sensitive enough to measure low abundance proteins, RNAs, and other biomarkers that could aid in the early and reliable diagnosis of cancer. There is a strikingly clear need to develop techniques capable of detecting biomarkers specific for breast cancer that will enable earlier diagnosis of disease, prediction of patient outcome, and improve therapeutic efficacy in a non-invasive manner. Our goals are to utilize ultrasensitive single molecule techniques developed in our laboratory to discover new biomarkers that meet these requirements within serum so that a simple blood test can be implemented. We are also working to characterize breast cancer biopsy samples with single cell resolution to discover the nature of the underlying heterogeneity in complex cell populations with the goal of correlating disease outcome with genotypes and phenotypes of individual cells.

BODY

David R. Walt, PhD, *Tufts University, Department of Chemistry 62 Talbot Ave Medford, MA 02155*

Task 1. Develop single molecule diagnostics using HIM (Human-in-Mouse) model (Years 1-2).

1a. Select approximately ten candidate markers (mt DNA, proteins, stem cell markers, etc.) in conjunction with collaborators (Months 1-6).

Upon discussion with Drs. Charlotte Kuperwasser, Rachel Buchsbaum, and other experts in the field, the previously mentioned list of protein biomarkers has been revised. Biomarkers previously selected that were later found to be present in healthy serum were eliminated from the list and several additional markers were included. The complete list is as follows: EGFRv3, ER-α, ADAM12, LALBA, β-casein, BAG3, BORIS, CD49f, CYR61, CDKN2D, CK8/18, DCTN3, GATA3, GRHL3, KLLN, KIFAP3, LCN2/NGAL, PMS2, PR, RRBP1, SERPINE2, SLUG, SNAIL, TBX3, VPSI3D, and VIM. Two additional markers, PSA and MCP-1, were also added as candidates to validate the mouse model since PSA has an established digital ELISA and MCP-1 has available antibodies suitable for sandwich ELISA.

1b. Develop single molecule assays for the candidate markers selected in 1a. Assays will be developed on microspheres and tested first on standard samples. Assay performance characteristics will be determined to ascertain that they will address concentration ranges of interest and requisite precision. For general protocols see: Nature Biotechnology, 2010, 28, 595-599 (Months 3-15)

Digital ELISA Development

In the past year, digital ELISAs have been developed for several protein biomarkers, including PR, ER-α, CYR61, LCN2, and MCP-1. Each developed assay lowered the detection limits of the respective bulk assay between 150-1,000X—a significant improvement in LOD. The following section describes the work performed for each biomarker.

Progesterone Receptor (PR)

PR is an estrogen-regulated gene that is overexpressed in up to 55–65% of breast cancers, known as PR-positive tumors (PR+). PR was demonstrated in several studies to have value as a prognostic and predictive marker in breast cancer.[6,7] To the best of our knowledge, PR has not yet been studied in serum. Since breast cancers of this subtype respond well to endocrine therapy, measuring elevated levels of PR within serum may aid in both diagnosis and patient treatment.

A bulk assay was developed for PR using antibodies acquired from R&D Systems. Capture antibodies were coupled to carboxyl magnetic beads using 1 mg/mL antibody and 1 mg/mL EDC. Pre-biotinylated detection antibody was used at a concentration of 0.2 µg/mL and 500 pM streptavidin β-galactosidase was used for enzymatic amplification. The bulk assay showed increasing fluorescence intensity with increasing protein concentration, as shown in Figure 1. The calculated LOD for the bulk assay was 1.3pM.

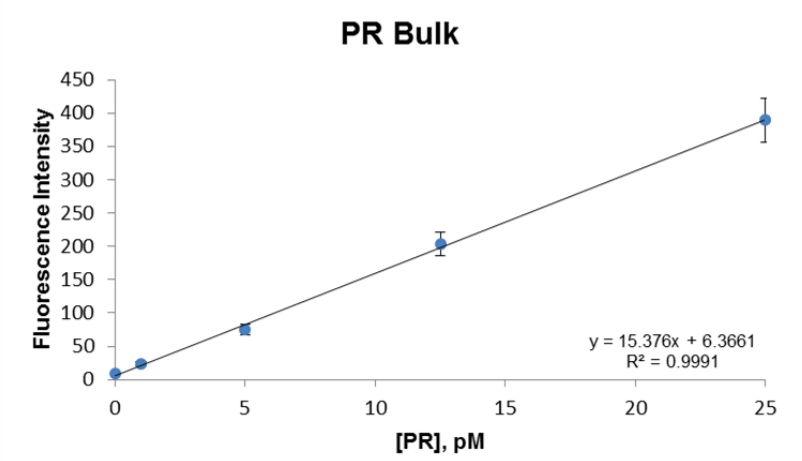

Figure 1: PR bulk bead assay using a microtiter plate reader with a gain of 50 and 500 pM sβg, LOD = 1.3 pM.

The successful bulk results indicated that the R&D Systems antibodies may be a good pair for a Digital ELISA assay. Digital ELISA assays were performed using beads coupled under the same conditions mentioned above—0.2 µg/mL detection antibody and 20 pM streptavidin β-galactosidase. Optimization showed that 50 pM of enzyme was an ideal concentration for the assay. Representative data from the optimized digital ELISA assay for PR is shown in Figure 2, where the LOD was ~1.5 fM. ***This decrease in the LOD represents almost a 1,000X increase in sensitivity over the bulk bead assay.***

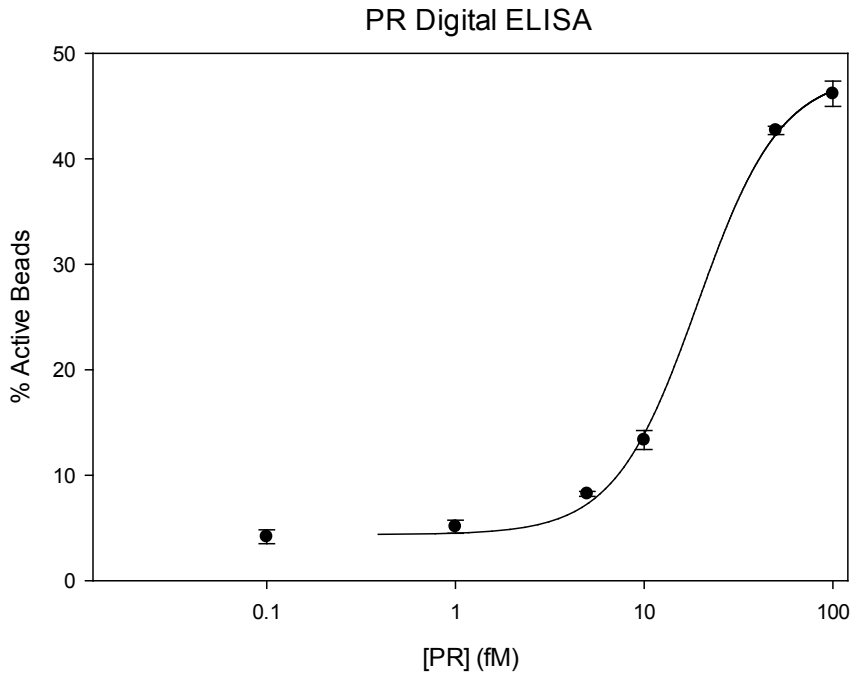

Figure 2: PR Digital ELISA assay with 50 pM sβg, calculated LOD = 1.5 fM.

Further optimization was attempted in order to further lower the detection limit. For example, attempts were made to conjugate additional biotin molecules to the pre-biotinylated detection antibodies. This approach however, led to unsuccessful bulk assays and Digital ELISAs were not attempted as a result. Different bead coupling protocols were also tried during this time, but no difference was seen between the two methods.

Estrogen Receptor-α (ER-α)

ER-α plays a critical role in reproductive physiology and bone remodeling. These vital receptors are overexpressed in up to 75% of breast cancers, known as ER-positive tumors (ER+).[7] Upon binding of estrogen, proliferation of mammary cells is stimulated. Thus, overexpression of ER-α leads to increased cell division and DNA replication, mutations, and eventually tumor formation. ER+ tumors tend to be well differentiated, less aggressive primary tumors and have a general better clinical outcome.[7] To the best of our knowledge, there is no evidence of measurements of ER-α in serum, but measuring elevated levels in serum may aid in diagnosis and treatment since tumors of this subtype respond well to endocrine therapy.

Figure 3 below shows data for a bulk assay developed for ER-α using antibodies acquired from R&D Systems. As was done for the PR bulk assay, magnetic beads were coupled with 1 mg/mL monoclonal capture antibody using 1 mg/mL EDC for the reaction. A concentration of 0.2 µg/mL and 500 pM biotinylated detection antibody and streptavidin β-galactosidase were used for the assay, respectively. The calculated LOD for the bulk assay was 1.2 pM.

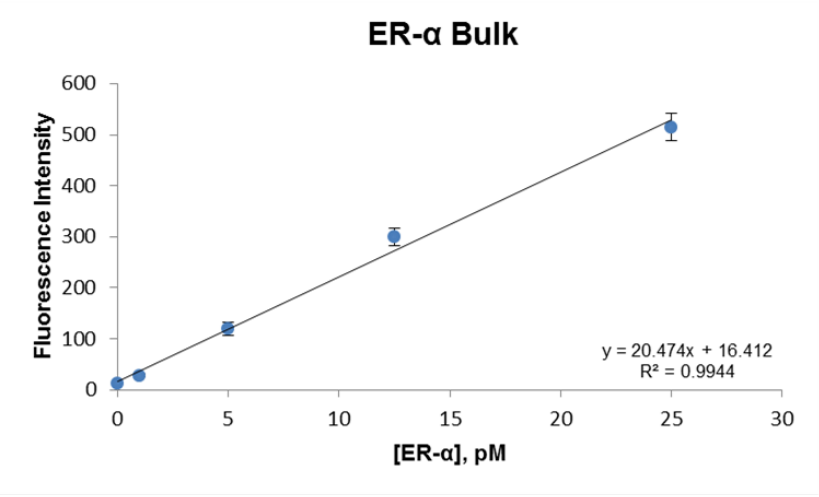

Figure 3: ER-α bulk bead assay using a microtiter plate reader with a gain of 50 and 500 pM sβg, LOD = 1.2 pM.

After the R&D Systems antibody pair was successfully validated in a bulk bead-based assay, a Digital ELISA assay was run using the same pair. The assay conditions were optimized to 20 pM β-galactosidase and 0.2 µg/mL detection antibody. The resulting calibration curve for the digital ELISA is shown in Figure 4. The calculated LOD was approximately 1 fM, ***which is about 1,000 times more sensitive than the bulk assay.***

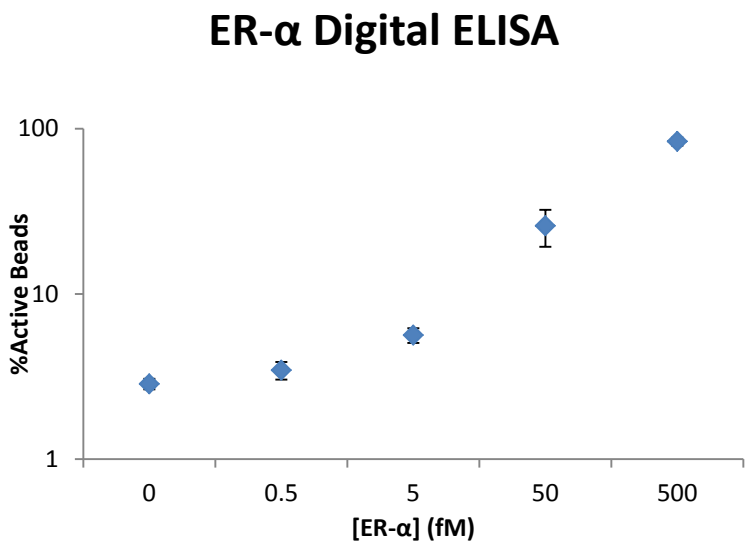

Figure 4: ER-α Digital ELISA assay with 20 pM sβg, calculated LOD ~ 1fM.

Monocyte Chemotactic Protein-1 (MCP-1)

MCP-1 is secreted in both immunoregulatory and inflammatory processes. It has been suggested that MCP-1 contributes to tumor malignancy in breast cancer.[8] MCP-1 is detectable in normal patient serum, but we aim to use this biomarker as a benchmark in the mouse model to examine the growth of human tumors within mice.

Figure 5 shows a bulk assay for MCP-1. Antibodies were acquired from Abcam. Similar conditions were used for coupling as previously described for PR and ER-α. Detection antibody was

biotinylated and was measured to have approximately eight biotins attached. The LOD for the bulk assay shown below was approximately 1.2 pM.

The corresponding digital ELISA assay for MCP-1 is shown in Figure 6. Although this assay was successful and had a calculated LOD of approximately 7 fM, optimization can further increase the sensitivity of this assay. Trying more combinations of antibodies is one possibility. The original antibody pair that was used for the assay was purchased from R&D Systems, due to previous success using antibodies from this company. Despite good results in the bulk range, the single molecule experiments were unsuccessful, even with optimization.

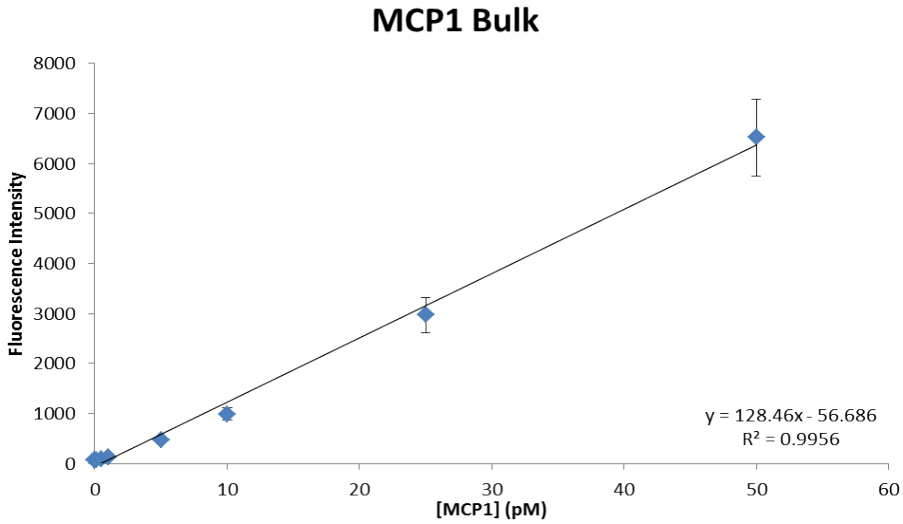

Figure 5: MCP-1 bulk bead assay using a microtiter plate reader with a gain of 50 and 150 pM sβg, LOD = 1.2 pM.

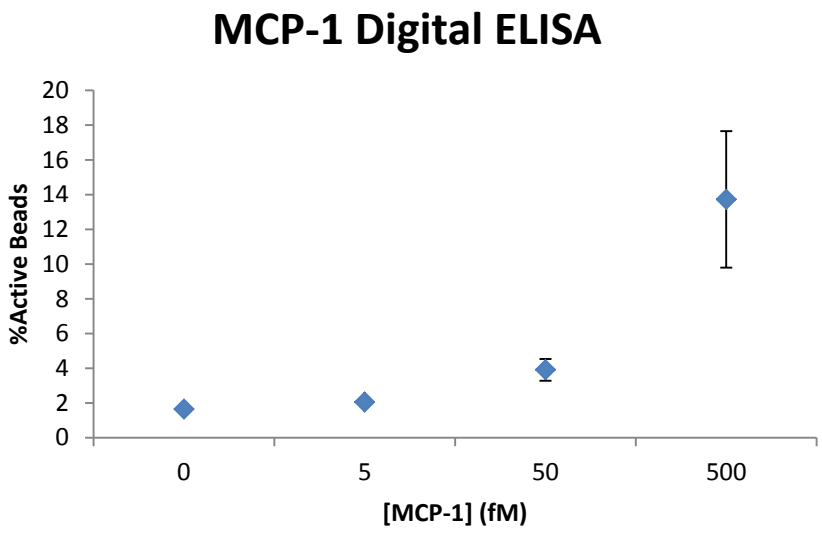

Figure 6: MCP-1 Digital ELISA assay s. A) Antibodies from R&D Systems, B) Antibodies from Abcam, LOD~ with 20 pM sβg, calculated LOD ~7 fM

Lipocalin-2 (LCN2)

Lipocalin-2 is an extracellular protein that binds ligands to present to cell surface receptors and other proteins to form macromolecular complexes, playing a role in cell regulation, proliferation, and

differentiation. Overexpression of this protein in breast cancer is associated with invasiveness, angiogenesis, disease progression, and lymph node metastasis. It has previously been detected in the urine of breast cancer patients[9], leading us to believe it will be detectable in serum using the Digital ELISA method.

Matched pair antibodies were purchased from R&D Systems, and a bulk assay was performed using the bead platform. Capture antibodies were coupled to microspheres and incubated with picomolar concentrations of LCN2 standard. The detection antibody was biotinylated in-house and was used at a concentration of 1.5 µg/mL, followed by 200 pM streptavidin β-galactosidase for the enzymatic readout. The bulk assay was a success, showing a positive linear response to increasing concentration of target protein and a LOD of 916 fM, shown in Figure 7.

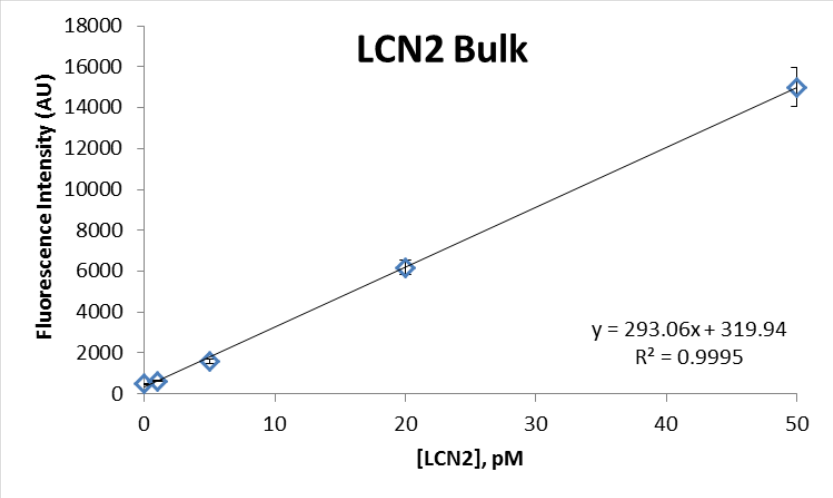

Figure 7 . LCN2 bulk bead assay using microtiter plate reader. [SβG] = 200 pM. Calculated LOD =916 fM.

Once the bulk assay was successfully established, conditions such as detection antibody and enzyme concentrations were optimized for single molecule studies. Figure 8 shows results from such a study, where the LOD was measured to be 1 fM. Detection antibody was used at a concentration of 0.05 µg/mL with 15 pM SβG used for the enzymatic readout. The femtomolar level assay proved to ***be ~1000 times more sensitive than the bulk assay*** shown Figure 7. Future work with this marker includes optimizing conditions to increase signal-to-noise ratio.

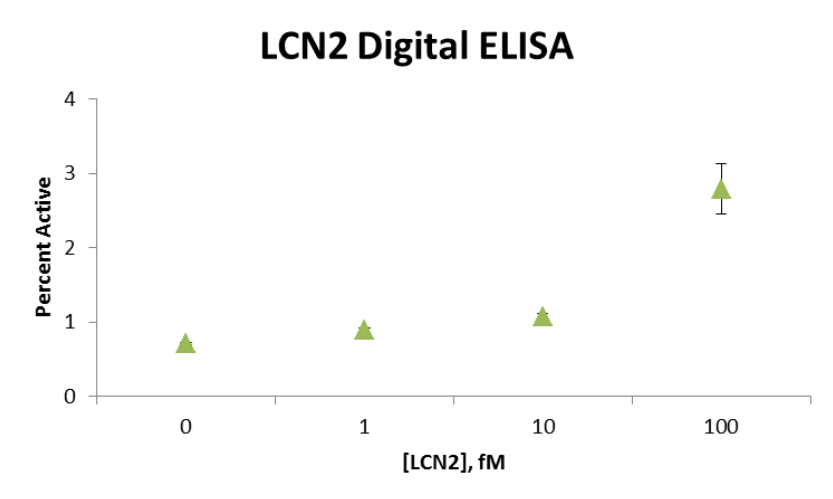

Figure 8. LCN2 Digital ELISA, [SβG] = 15 pM. Measured LOD = 1 fM.

Cysteine-Rich Angiogenic Inducer 61 (CYR61)

Cysteine-rich angiogenic inducer 61 (CYR61) is a secreted, extracellular matrix associated protein known to regulate cellular proliferation, migration, angiogenesis, and survival. CYR61 has been linked to ER negativity, as well as more aggressive breast cancer types.[10,11] To the best of our knowledge, there have been no reports of CYR61 detected in the blood of breast cancer patients.

Antibodies were purchased from R&D Systems and tested in a bulk assay format using antibody-coated microspheres for target capture. As done previously with LCN2, anti-CYR61 beads were incubated with varying concentrations of CYR61 standard, tagged with biotin-labeled detection antibody, and detected using enzymatic readout. This bulk assay was also a success, showing increased signal in response to increased concentration of target in solution. The limit of detection could not be calculated using the linear curve generated from the data, but the measured limit of detection was 1 pM, shown in Figure 9 below.

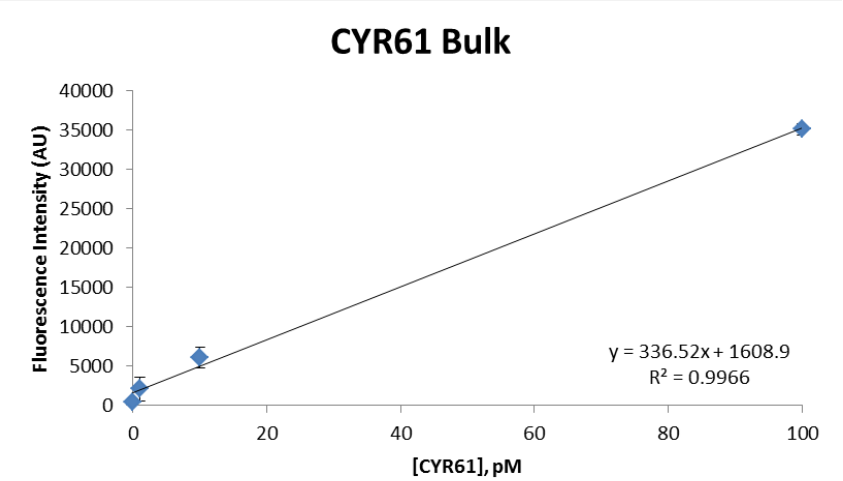

Figure 9. CYR61 bulk bead assay using microtiter plate reader, [SβG] = 200 pM. Measured LOD = 1 pM.

Conditions for the assay were then varied in order to facilitate consistent single molecule detection. This particular assay proved to be more difficult to optimize with a much higher background signal, shown below in Figure 10. The overall low response coupled with high variability has resulted in a relatively high measured LOD of ~50 fM, a 20x improvement from the bulk bead assay. Future work will involve optimizing the assay to decrease variability and increase overall signal with minimal impact on the background.

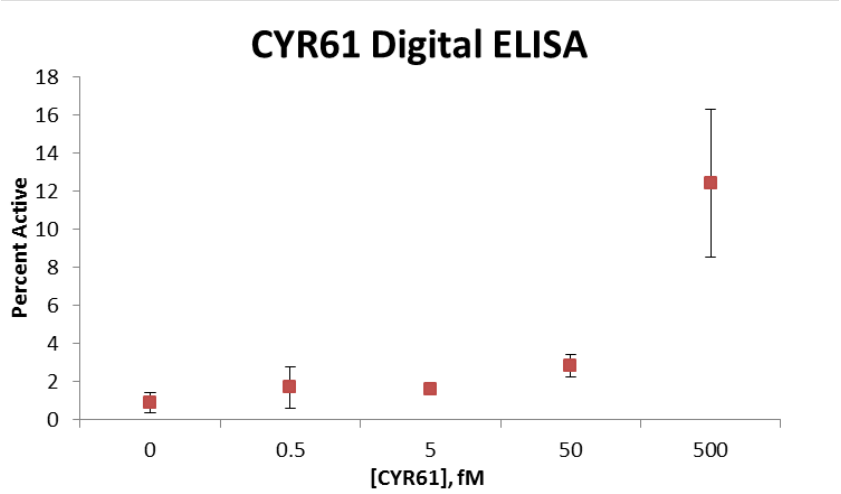

Figure 10. CYR61 Digital ELISA, [SβG] = 15 pM. Measured LOD = 50 fM

Several other assays are currently under development, although to date they have shown limited success in the bulk assay stage. These markers of interest include TBX3, LALBA, BORIS, Vimentin, CDKN2D and GRHL3. Matched antibody pairs are not commercially available for the majority of these markers, so antibodies have been purchased from various manufacturers and are being tested on the bead platform in bulk. We are aggressively pursuing other options for binding reagents to the biomarkers of interest. Custom antibodies and FN3 monobodies are also being pursued as options to generate binding pairs with sufficient affinity for a sandwich ELISA format. Additionally, the Kay lab at the University of Illinois at Chicago is in the process of producing FN3 monobodies for TBX3 and BORIS, while Abnova has screened and paired their available antibodies for TBX3 detection. Somalogic is currently creating Somamers for several biomarkers as well, including RRBP1, BORIS, VIM, TBX3, LALBA, GRHL3, and KIFAP3.

1c. Screen blood samples from 'Human-In-Mouse' (HIM) Model obtained from Kuperwasser (Months 12-24). HIM tumors will be created from human breast epithelial cells collected from discarded tissues of women who have undergone reduction mammoplasty surgeries. For more information/details on model: *Nature Protocols*, 2006, 1, 595-599.

Since several of our assays were developed with sufficient LODs in the digital range, the Kuperwasser lab ran several mouse cell line-based xenograft studies. Approximately one million cells of an appropriate breast cancer cell line were injected into the mice. Upon tumor formation, terminal bleeds were extracted from the mice and the serum was sent to our lab for biomarker testing. The assays we tested first were PR, ER-α and MCP-1.

PR is overexpressed in the breast cancer cell line T-47D (ATCC HTB-133), which is a human epithelial cell line originating from a metastatic site on the mammary gland. Figure 11 shows data derived from two T-47D mouse serum samples. Sample 607 came from a mouse with a 2 mm sized tumor and sample 612 was from a mouse with a 1 mm sized tumor. The samples were run in conjunction with a protein standard for calibration. There appears to be no difference in the two samples, but there is measurable PR within the two samples above the blanks and lower concentration standards. The calculated concentrations for the two samples were 11.4 and 10.8 fM of PR, respectively.

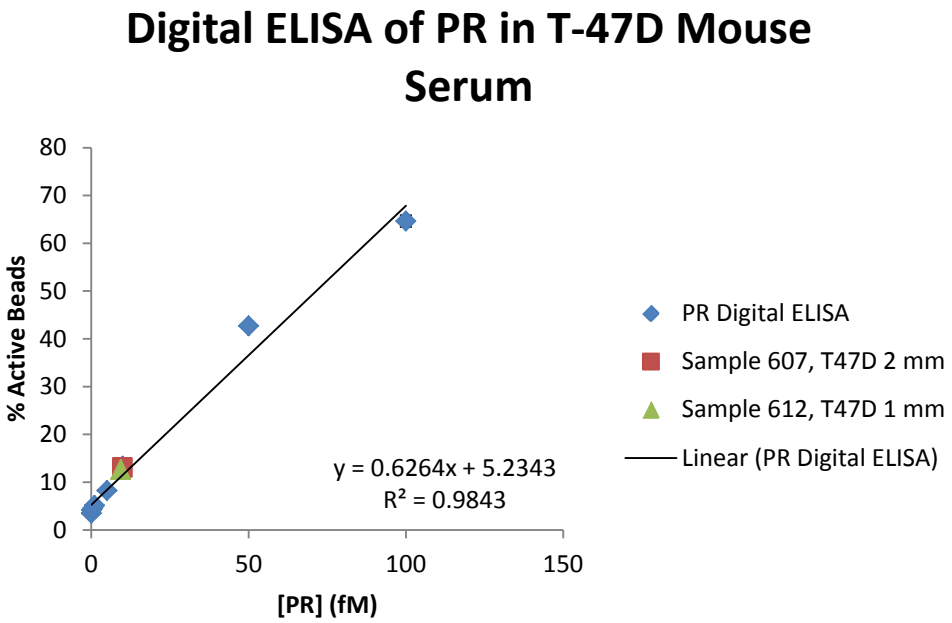

Figure 11. Digital ELISA for PR was used to measure mouse serum from T-47D cell line tumors. Samples 607 and 612 measured 11.4 and 10.8 fM PR, respectively. Serum was diluted to 25% in PBS.

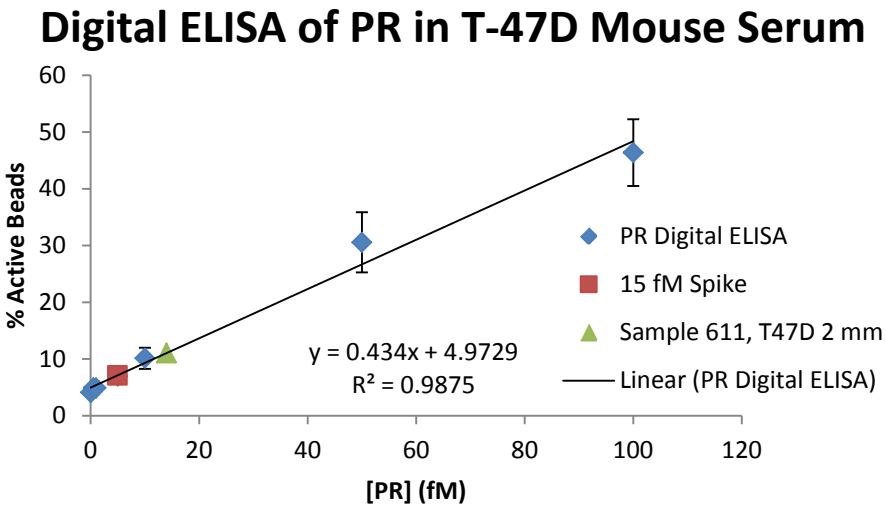

Figure 12. Digital ELISA for PR was used to measure mouse serum with T-47D cell line tumors. Sample 611 measured 14 fM. Serum was diluted to 25% in PBS. The 15 fM spike measured 4.93 fM ER-α, making the spike recovery only ~33%.

When the experiment was repeated (Figure 12), however, using another 2 mm tumor (Sample 611) and a 15 fM spike, the sample was calculated to have 14 fM PR, but the 15 fM spike only measured 4.93 fM, or a ~33% recovery. Upon speaking with collaborators, it was thought that this problem could be due potentially to some interference with the mouse serum i.e. some of the PR might be clustered, and it needs to be diluted more. The aforementioned experiments were performed using 25% mouse serum. We

are currently waiting for more samples from the Kuperwasser lab in order to test this theory and examine more samples.

Work on the ER-α assay was also examined in mouse serum using the MCF7 (ATCC HTB-22) cell line for the xenografts,, which is known to overexpress ER-α. Figure 13 shows the digital ELISA results from measurements of two samples, serum from a 2.5 mm tumor and serum from a 7.5 mm tumor. As shown in the graph, both samples displayed similar levels of ER-α, 6.7 fM and 7.1 fM for the 2.5 and 7.5 mm tumors, respectively. The 50 fM spike also showed results of ER-α with a reading of 7.7 fM. The recovery for this experiment, according to the spiked sample, was approximately 14%. All of the samples were diluted to 25% in PBS. Similar to the PR experiments above, it was suggested that the ER-α was sequestering and future experiments should use higher dilution factors.

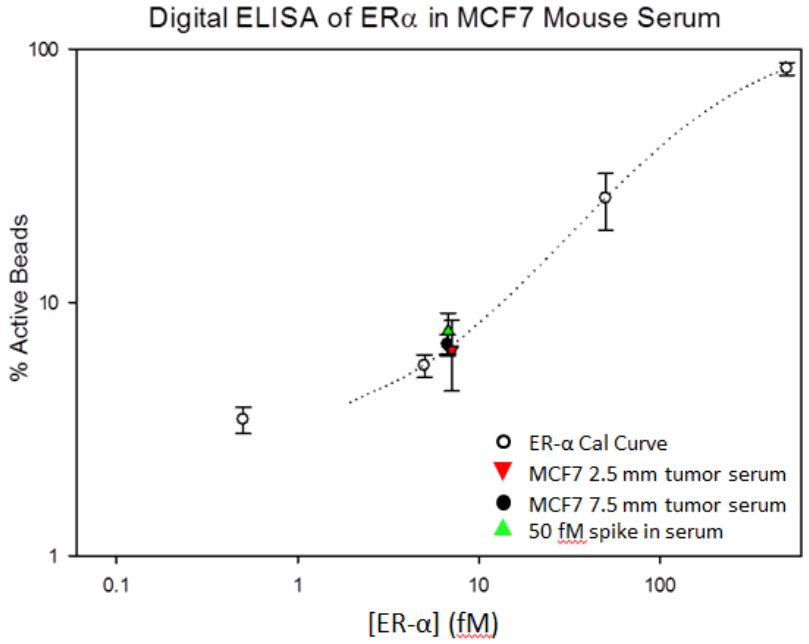

Figure 13. Digital ELISA measuring ER-α in mouse serum with MCF7 cell line tumors. Two tumor samples were measured, one with a 2.5 mm tumor and one with a 7.5 mm tumor. The ER-α concentration in the samples was 6.7 and 7.1 fM, respectively. The 50 fM spike measured 7.7 fM ER-α, making the spike recovery only ~14%.

Per the request of collaborators, calibration curves were established for ER-α comparing the standard assay buffer, QBlock, which is comprised of PBS and Newborn Calf Serum, and healthy control mouse serum. Figure 14 shows the resulting calibration curves for the two media. It is evident from the curves that mouse serum does not interfere with the protein standard and thus the spikes should be an accurate representation of the concentration of protein present in the sample. Murine serum samples were also run with these two calibrations; however, no detectable signal was seen within the samples.

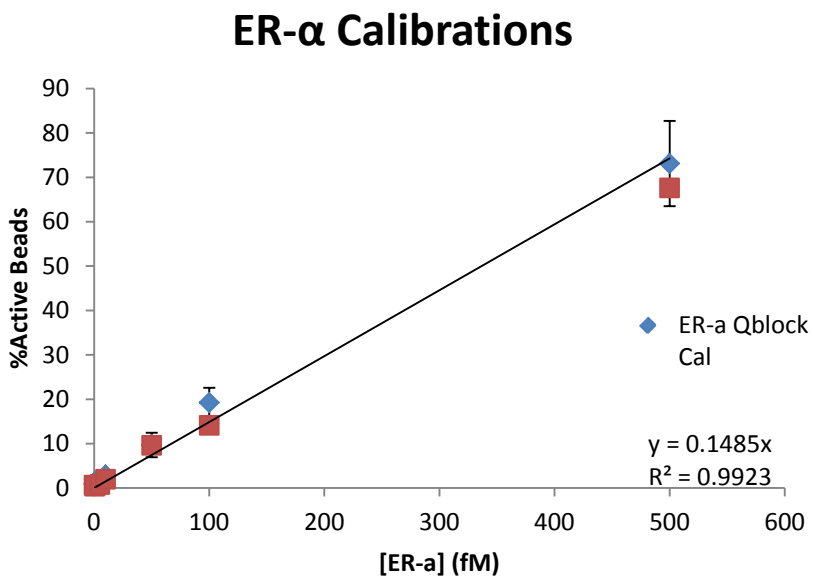

Figure 14. Digital ELISA measuring ER-α using both QBlock (25% Newborn Calf serum in PBS) and 10% control mouse serum in PBS. The two calibrations show there is no difference between the recovery of ER-α in mouse serum compared to the standard QBlock buffer.

Mouse samples have also been obtained that are positive for MCP-1. So far, digital ELISA has not been able to detect any MCP-1 within the samples. This lack of detection may be because the assay is not yet sensitive enough for the low levels of MCP-1 that exist in the serum. More assay optimization will be performed before experimenting further with serum samples.

The Kuperwasser lab is also currently preparing mice that will bear tumors from the LNCaP (ATCC CRL-1740) line. This cell line originates from the prostate and will produce prostate specific antigen (PSA). Although this marker may not seem applicable to a breast cancer study, one of the most sensitive digital ELISAs was developed for PSA. Our goal is to establish a proof-of-concept that the Digital ELISA can detect cancer biomarkers in mouse blood from appropriate cell lines. It is hoped that the high sensitivity of the PSA assay will allow us to obtain positive results in mouse serum, and improve our ability to begin to move to human samples.

Task 2. Apply single molecule diagnostic technique (developed in Task 1) to analysis of human serum samples (Years 3-5).

2a. Screen clinical samples obtained from Buchsbaum for presence of the markers that could be detected in HIM model (Months 25-30).

These studies have not been initiated per SOW.

2b. Iterate 2a-2d until a sufficient number of markers has been identified for further investigation. Some candidate markers are expected to either not be found in the clinical samples or will not be predictive of disease state. Other markers may be difficult to measure due to lack of suitable binding reagents. As these markers drop out, others will be added to ensure there is a sufficient number when sample set is expanded (2c) (Months 25-48).

These studies have not been initiated per SOW.

2c. Expand sample set and run clinical samples with all assays developed for all markers (Year 5).

These studies have not been initiated per SOW.

2d. Determine which markers in blood correlate with disease using data processing and computational methods available in the laboratory (Year 5).

These studies have not been initiated per SOW.

Task 3. Develop single cell analysis methods to determine composition of a primary tumor.

3a. Select approximately ten candidate markers (SNPs, proteins, etc.) of value for single breast cancer cell analysis in conjunction with collaborators (Months 1-9).

We have also chosen to utilize the pre-established PSA assay to validate our assay at the single cell level. This assay has proven to be extremely sensitive and our goal is to take advantage of the sensitivity of this established assay while we work on gaining single cell resolution.[12] In order to test this assay within cells, we began culturing LNCaP cells, courtesy of the Kuperwasser lab. We have also performed work towards developing single cell assays using the PR digital ELISA assay we established in the lab. For this assay, we began culturing T-47D cells (courtesy of the Kuperwasser lab), which overexpress PR.

3b. Detect presence of mtDNA by screening for many sequences using cultured cell lines and HIM tissue samples to select which markers to use. Will require development of mtDNA microarrays and sample screening (Months 6-18).

The selection of mtDNA markers is being performed in conjunction with the Sonenshein laboratory (see Sonenshein Task 1 below). The DNA assay developed above in Task 2 will be the basis for the assays we plan to use for Tasks 3b and 3c.

3c. Develop assays for the selected markers (Months 6-24).

As previously mentioned, the Digital ELISA assay for PSA has already been developed. Figure 15 shows a digital ELISA assay we performed, demonstrating that our capture beads and detection antibodies work sufficiently and that our assay was also successful. The assay was run using 20 pM streptavidin β-galactosidase and 0.2 µg/mL detection antibody. The digital ELISA assay for PR can be seen above in Figure 2.

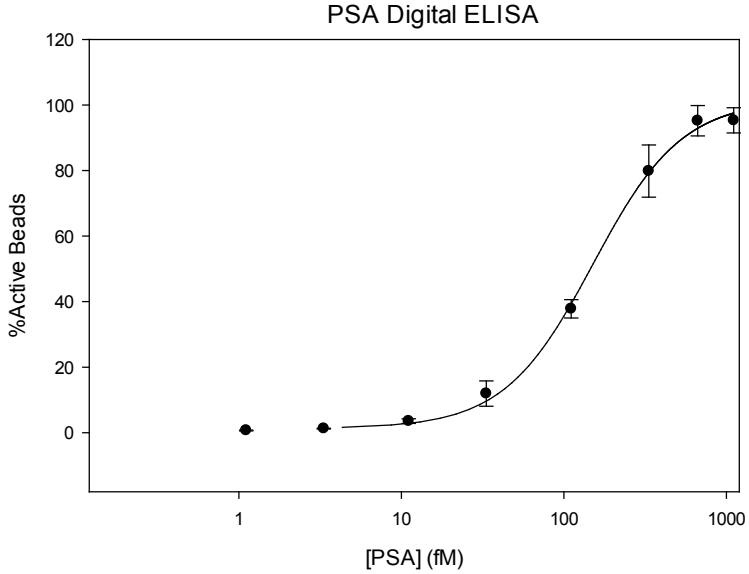

Figure 15. Digital ELISA calibration curve for PSA. [SβG] = 20 pM.

3d. Develop single cell assays for selected markers (Months 18-36).

For single cell assay development, the current digital ELISA protocol needed to be optimized. In order to not dilute the low concentrations of protein contained within individual or low numbers of cells, we chose to decrease our assay volume from 100 µL to 10 µL for target incubation. The number of beads used is also reduced from 500,000 to 100,000 in an attempt to decrease excessive dilution of the target amongst a vast number of beads. Several other combinations of assay working volumes and bead numbers were also tried, but this combination has proved to work the best so far. Generally, cells are diluted and counted, and 1 µL of cells is added to a well in a PCR plate containing beads and 9 µL of lysis buffer. The cells are then lysed in the presence of the beads, and the contents are captured for downstream digital ELISA.

Figure 16 shows an experiment measuring PR in low numbers of T-47D cells. There is high variation between measurements due to the need to perform a bead transfer after lysis and capture as well as an overall lower number of beads used in the assay. We were able to measure PR in 100 cells, but the concentration of PR in 10 cells approaches the lower limit of the assay. The measured PR concentrations for 10 and 100 cells were 7.35 and 94.4 fM, respectively. Samples containing 1000 cells were also examined, but are not shown on the chart because the measurements were well beyond the range of the calibration curve, as shown in the chart inset in Figure 16.

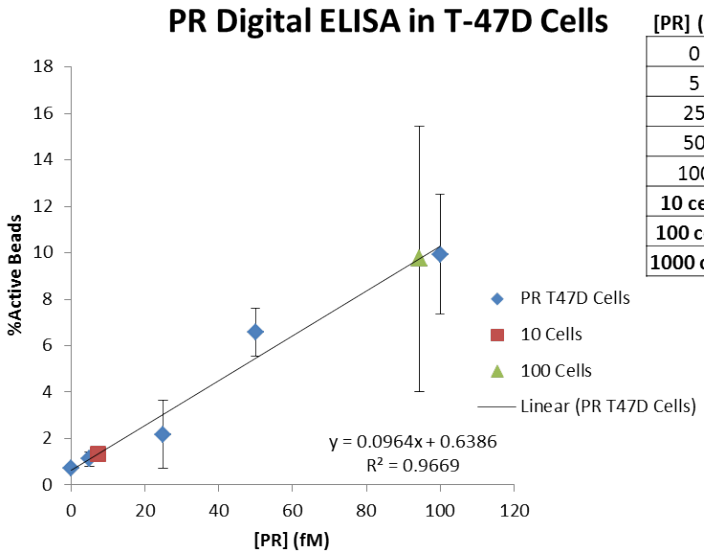

[PR] (fM)	%Active	Stdev	
0	0.72	0.14	
5	1.13	0.31	
25	2.18	1.47	
50	6.57	1.04	
100	9.93	2.57	[PR] (fM) Calculated
10 cells	1.35	0.27	7.35
100 cells	9.74	5.72	94.41
1000 cells	52.76	6.80	540.68

Figure 16. Digital ELISA for PR in T-47D cells. The reading for 10 cells is on the border of the LOD for this assay. PR is detectable in 100 cells, with a concentration of 94 fM.

The LNCaP cells were examined in a similar method to the T-47D cells. Figure 17 shows data examining the PSA content of dilutions of 5, 10, 100 and 800 LNCaP cells. According to this data, the PSA content of 10 cells, ~2 fM, was above the assay detection limit. This is a clear improvement over the PR assay. The measurements of only 5 cells, however, seemed to reach the detection limit. In order to improve our sensitivity and enable single cell resolution, we intend to continue to modify the reaction conditions of the single cell digital ELISA. These modifications include assay volume, bead numbers, incubation time, etc.

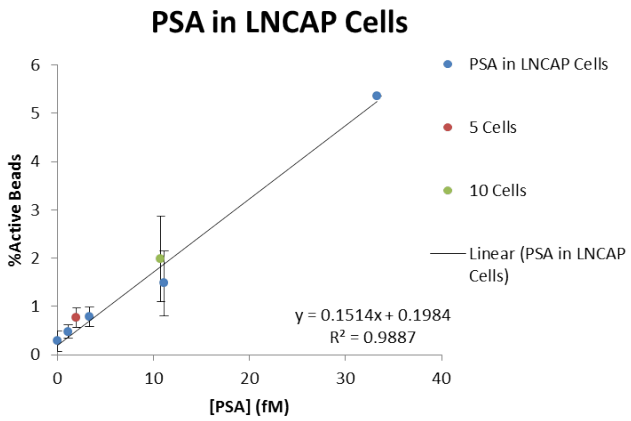

[PSA] fM	Avg. %Active	StDev of %Active	
0	0.28	0.21	
1.11	0.48	0.13	
3.33	0.79	0.20	
11.1	1.48	0.67	
33.3	5.36	0.00	
111	17.10	4.13	
333	46.05	5.99	**[PSA] (fM) Calculated**
5 cells	0.77	0.21	1.96
10 cells	1.98	0.88	10.74
100 cells	21.55	5.12	152.42
800 cells	79.07	18.57	568.95

Figure 17. Digital ELISA for PSA in LNCaP cells**.** PSA is detectable down to 10 cells, with an average PSA content of 10.74 fM.

3e. Obtain tissue samples from HIM (Kuperwasser) and perform single cell analysis (Months 36-48).

These studies have not been initiated per SOW.

3f. Determine if one can observe rare cells with more aggressive genotypes or protein levels in HIM samples (Months 42-54).

These studies have not been initiated per SOW.

3g. Confirm presence of the single cells in human breast cancer biopsy samples obtained from Buchsbaum (Months 48-60).

These studies have not been initiated per SOW.

Daniel T. Chiu, PhD, *University of Washington, Seattle Campus Box 351700 Seattle, WA 98195-1700*

Task 1. Work with Walt lab to develop/refine single-molecule and single-cell techniques for analyzing protein and cell biomarkers (Months 1-36).

Task 1 *will use cultured cell lines, commercially available serum samples, and serum samples from HIM model.*

For Task 1, we have made excellent progress towards the detection and analysis of cell biomarkers, in particular, circulating tumor cells (CTCs). CTCs have emerged as an important and valuable biomarker for the prognosis of breast cancer, and the sensitivity we have demonstrated makes CTCs a robust biomarker for prognosis and as an indicator of treatment efficacy. The high sensitivity has also the potential to make CTCs a diagnostic tool if they are present at sufficient levels in blood. Below, we describe each subtask in more detail.

1a. Develop microfluidic devices for sample preparation and optical manipulation. Initial devices will contain only sample preparation module for use by Walt lab (Years 1-2).

Last year, we reported on the successful development of a CTC analysis method called ensemble-decision aliquot ranking, or eDAR, which combined the following components: multi-color line-confocal fluorescence detection with a high sensitivity, a hydrodynamic switching mechanism, a cell trapping and subsequent purification process, and an identification and downstream analysis section. It had a high throughput, analyzing 1 mL of whole blood in 20 minutes, with over 90% recovery ratio and a zero false positive rate. CTCs were captured onto a very small area (1 mm^2) with a high enrichment ratio. Although

eDAR was more sensitive than the CellSearch method, which is currently the only FDA approved system for CTC enumeration, in detecting CTCs from metastatic breast cancer patients; the original version of eDAR still has several factors that limit its clinical application. The original microchip had six layers, which constrained the yield and efficiency of the chip production. Although the throughput of fluorescence imaging was greatly improved because of the very small area on which CTCs were trapped, the imaging quality could be adversely affected by the track-etched filter, generating a non-uniform background.

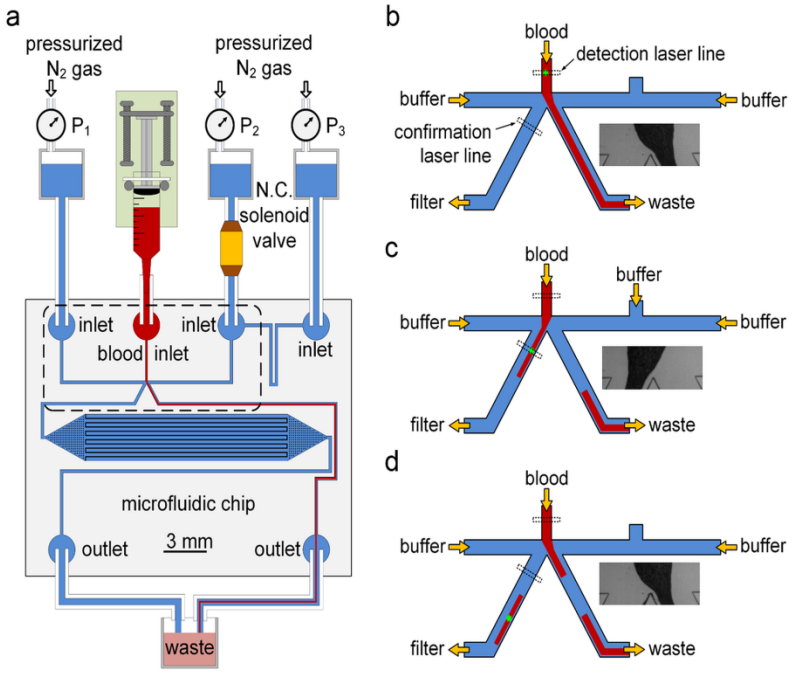

Figure 18. Microfluidic chip and hydrodynamic switching scheme of the second generation eDAR. a) General structure of the microfluidic chip and the configuration of the eDAR platform. The bottom left channel was designed to collect sorted aliquots and transfer them to the subsequent purification area, which had 20,000 microslits. The area marked with a dashed box is further explained in b-d. b) The flow condition when no positive aliquot was ranked. c) The blood flow was switched to the CTC collection channel, and the sorted aliquot was confirmed by the second APD. d) The blood flow was switched back after the aliquot was sorted.

To address these issues so we are in a position to translate this technology to clinical applications, we have successfully developed a second generation of eDAR, which included an integrated filtration area fabricated by standard lithography methods (Figure 18). This microchip had only two layers of feature on the silicon master and could be fabricated with one-step replica molding into polydimethylsiloxane (PDMS) and then bonding to a glass substrate. The entire system was also simplified with a new active sorting scheme. We carefully evaluated several different designs of the microfluidic chip and hydrodynamic switching mechanisms, and optimized the analytical performance of the device. The recovery efficiency was 95% with a zero false positive rate (n=15), and the highest throughput tested was 4.8 mL of whole blood per hour.

There are two key factors that determined the feature and performance of an eDAR platform: an efficient and active sorting scheme and a subsequent efficient purification scheme. Here, we designed the second generation of eDAR-platform to optimize these two components. Below, we briefly summarize the improvements we achieved.

Redesigned Hydrodynamic Sorting Scheme. In the first generation of eDAR, we designed a mechanical valve to control the active sorting step, which was fast (about 2 ms response time) and robust compared to other reported switching mechanisms. Although promising, some design factors of this mechanical valve scheme constrained the potential application of eDAR. To form the mechanical valve on the chip, 3 individual structural layers were required—the solenoid, its PDMS thread, and the microchannels on a 150-μm PDMS film. This would make the chip preparation complicated and time-consuming. Another shortcoming is the direct contact between the captured blood aliquots and the mechanical valve, which increased the risk of the loss or damage of CTCs. To overcome these issues, we replaced the solenoid with an off-chip model, which is normally closed but can be opened in 2 to 3 ms

when a 5V DC voltage is applied. Because this in-line solenoid was not a part of the microchip, the preparation of the microfluidic device was significantly simplified. The solenoids could be easily connected with any microchannels, so we could test many possible hydrodynamic sorting schemes. We designed and tested 8 different schemes (Figure 19) to drive the fluidic switch. Because of the structure of this type of solenoid and the elastic nature of PDMS, the fluidic performance varied a lot (Table 1), and we had to characterize each scheme to choose the one that offered the best performance.

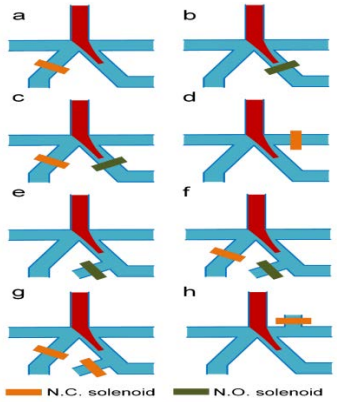

Figure 19. Eight hydrodynamic sorting schemes. The blood was injected from the main channel, shown as the red flow. Buffer (Blue) flowed in the two side channels, CTCs were collected to the bottom left channel, and the waste was directed to the bottom right channel. The rectangular block represents the solenoid. If the solenoid was set to be normally open (N.O.), the color of the block is set to green; if the solenoid was set to be normally closed (N.C.), the color is set to orange. See table 1 for more information.

After characterization and optimization, the structure of the platform and the corresponding scheme of the hydrodynamic sorting were chosen as depicted in Figure 18. The labeled blood sample was injected into the top channel of the chip using a syringe pump (Figure 18a). Two side channels, where buffer flowed through, were used to control the active sorting step. There were two ports placed on the right-side channel, and both of them were connected to a pressurized buffer source. The normally closed solenoid was connected to the port near the sorting junction to control the hydrodynamic switch. There were two channels after the sorting junction. The one on the left was used to collect positive aliquots and deliver them to the filtration and collection area for further purification; the one on the right was the waste collection channel where all the negative aliquots flowed through.

Scheme	Position	Normal state	Left pressure (psi)	Right pressure (psi)	Switch over time (ms)	Switch back time (ms)
a	Collection	Closed	Low	High	~2-3	~15-25
b	Waste	Open	High	Low	~15-20	~2-3
c	Collection	Closed	Low	High	~4-5	~10
	Waste	Open				
d	Right Buffer	Close	Low	High	~3	~40
e	Waste	Open	High	Low	~25	~2
f	Collection	Closed	Low	High	~25	~5-6
	Center Waste	Open				
g	Collection	Closed	Low	High	~2-3	~2-3
	Center Waste	Closed				
h	Center Right Buffer	Closed	Low	High	~2-3	~2-3

Table 1. Summary of the fluidic configuration and performance of the eight sorting schemes we tested. Two solenoids were used in schemes c, e, and g. When there were two outlets or inlets on a single channel, the position of the solenoid was marked. For example in scheme f, the position of the second solenoid was "center waste", meaning that it was placed on the center outlet of the waste collection channel. In every scheme, except g, when the "positive" events were detected, the DC voltage applied on the solenoids immediately was changed to trigger the sorting, and after a certain period of time was changed back to the normal state. Scheme g utilized four individual steps to control the sorting. Initially, both solenoids were set to closed, and the blood flowed to the waste channel. When the sorting was triggered, only the solenoid on the collection side was opened to perform the switch-over step; after the cell was collected, the other solenoid was opened to perform the switchback step. After the blood flow was completely switched back, both solenoids were closed at the same time, same as the normal state.

When those aliquots were ranked as "negative" (Figure 18b), there was no voltage applied on the solenoid so it was closed. An initial pressure drop was set between the No.1 and 3 buffer sources in Figure 18a, so the blood could only flow into the channel that collected the waste, which is also shown in the bright field image in Figure 18b. When a positive event was detected by the first detection window, a 5V DC voltage was immediately applied on the solenoid to open the buffer flow from the No.2 buffer reservoir. This decreased the flow resistance of the buffer channel on the right side and generated a higher flow rate there. The blood flow was pushed from the right side to the left to collect the positive aliquot (Figure 18c). After this aliquot was collected and confirmed by the second detection window, the solenoid was closed to switch the blood flow back to the waste collection channel (Figure 18d). The time required for the switch-over and back was determined to be 2 to 3 ms for each. This process was stable enough for eDAR even after more than 10^5 on-off cycles that we tested. The in-line solenoid was placed on the buffer line so blood could not come into contact with the solenoid, which eliminated the possibility of the blood-coagulation and cross-contamination. Moreover, in this scheme, there was a constant flow of buffer in the CTC collection channel during the eDAR process. This improved the efficiency of the subsequent purification step and prevented the formation of aggregates of cells.

Design and optimization of the further purification mechanism. In the first generation of eDAR, we used a piece of track-etched polycarbonate filter to retain and purify the captured CTCs. However, it required two additional layers in the micro-chip, as well as a complicated procedure to bond the filter to the PDMS. Here, we developed a new scheme of on-chip filtration based micro-slit structures, which were made of PDMS and did not require additional layers. Figure 19a shows the basic structure of these microslits, which captured the CTCs without retaining any red blood cells (RBCs). The size of the slit was optimized to be 5-μm tall and 5-μm wide (Figure 19b), which is smaller than the ones used in most of the CTC methods based on filtration. With this size of microslits, we minimized the risk of losing small CTCs, while still allowing many WBCs to deform and pass through the filter. Because the micro-filter was made of PDMS and bonded with a piece of coverslip, the imaging quality was improved significantly (Figure 19c and 19d) compared to the polycarbonate filter, which is not fully transparent and may cause scattering and aberration. Moreover, because the cells could only be trapped along the array of slits, they could be easily referenced and tracked; in many other methods, the cells are distributed randomly on the surface. This trapping along the slits made the imaging procedure faster and the results of enumeration more accurate. The slits also made it faster and more efficient to perform the secondary labeling on the trapped CTCs. Figure 19e shows that two breast cancer cells labeled with anti-EpCAM-PE were trapped on the microslit. We fixed, permeabilzed, and labeled them using anti-Cytokeratin-Alexa488, anti-Her2-Alexa647 and Hoechst. Fluorescence images showed the expression of these markers on these two cells clearly, and the bright field image also confirmed their morphology. We also labeled these two cells with anti-CD45-Alexa700 as a negative control marker, and did not find any signal from the color channel that corresponded to this tag.

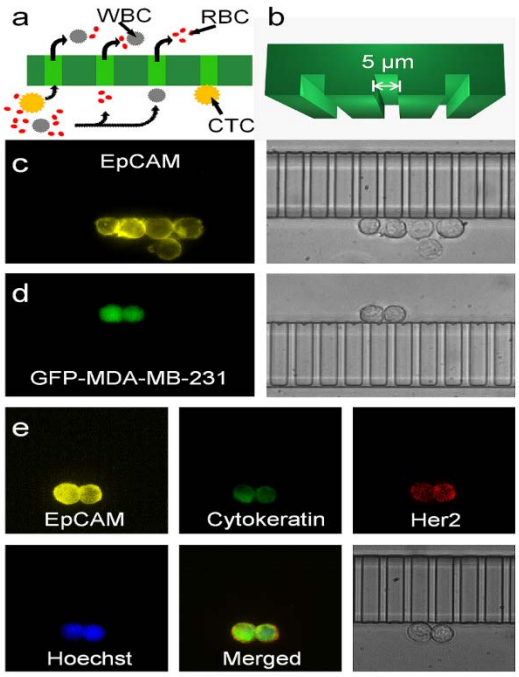

Figure 19. Microslits and multicolor fluorescence imaging of captured CTCs. a) The sorted aliquots were further purified through the array of microslits. Objects in yellow represent CTCs; red and grey objects represent RBCs and WBCs, respectively. The curved arrows show the flow paths across the microslits. b) The 3D model of the microslits with a 5-µm height and a 5-µm width. c) Fluorescence (left) and bright field (right) images of five breast-cancer cells (MCF-7) captured via eDAR. d) Fluorescence (left) and bright field (right) images of two MDA-MB-231-GFP cells (model cell line for triple-negative breast cancer) captured based on their GFP signal without any prelabeling. E) Two SKBr-3 breast cancer cells were captured by eDAR, and further labeled with additional markers.

To optimize the performance, we prepared and tested microchips with 1000, 5000, and 20,000 microslits. These chips helped us to determine the flow resistance across the filtration area, which could affect the hydrodynamic switching and the stress on the trapped cells. The eDAR-chip with 20,000 slits required a low pressure (< 4 psi) on the two side-buffer channels to balance the hydrodynamic switching process. The pressure drop across the microfilter was also lower, which would minimize the stress and deformation of the cell.

Characterization and analytical performance of eDAR. The efficiency of the active sorting step was monitored in real time. Figure 20a shows a small portion of the APD data from a cancer sample. The signals in blue were from the first detection window that ranked the aliquots and controlled the sorting. The two peaks at 978 and 1298 ms represented two CTCs labeled with anti-EpCAM-PE that triggered the aliquot sorting. The two peaks in red show that two cancer cells flowed through the second detection window located on the collection channel, confirming that the two positive aliquots were actually sorted. It is worthwhile to point out that the background change from the second detector (Figure 20a) also confirmed that only a small portion of blood was collected by eDAR, contributing to the high enrichment ratio of CTCs (up to a million fold for a typical sample).

Because the labeled CTC had to flow from the first detection window to the second one, we could observe a time difference between the decision APD peak and its confirmation signal. This time difference was defined as the transit time of the sorted CTCs, which might vary because the CTCs can have different linear flow rates due to the nature of laminar flow in the microchannel. Figure 20b shows the distribution histogram of the transit time at flow rates of 40 and 80 µL/min. Generally, a higher volumetric flow rate of the blood resulted in a shortened transit time of the sorted CTCs (Figure 20c). When the flow rate was 90 µL/min, the average transit time was lowered to 4 ms, very close to the switching time of the sorting scheme (2 to 3 ms), which implies that this is the limit for the throughput for this design of eDAR.

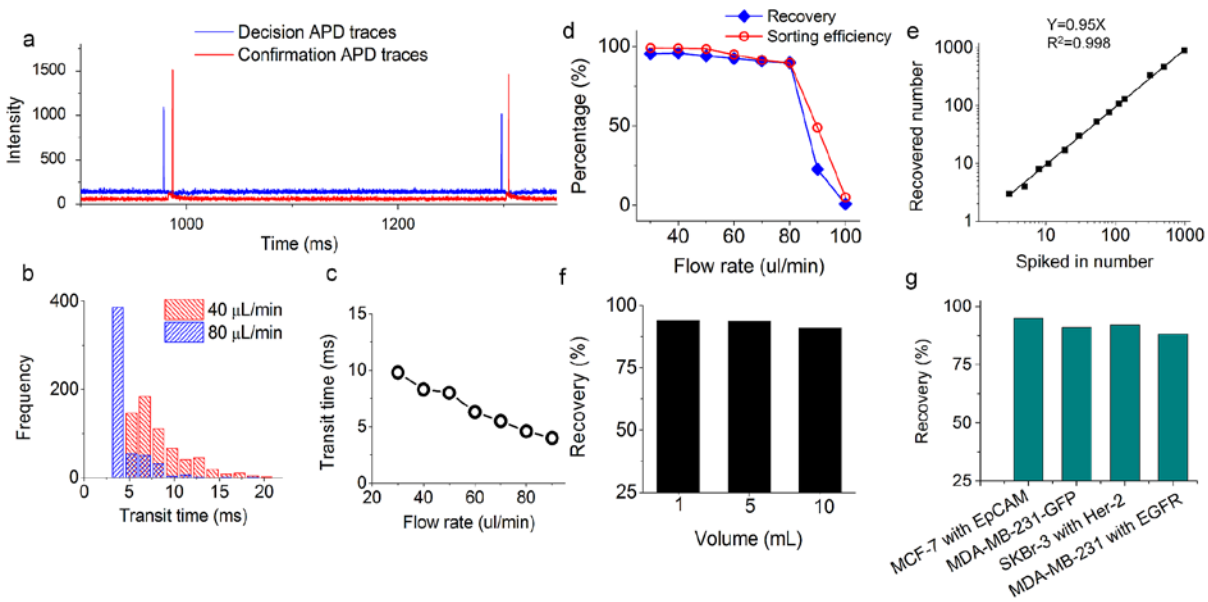

Figure 20. Characterization and analytical performances. a) The segment of the APD data from a cancer sample that shows two events triggered the sorting which then were confirmed by the second detection window. b) The distribution of transit time at flow rates of 40 and 80 µL/min, respectively. c) A plot shows the fastest average transit time was about 4 ms when the flow rate was 90 µL/min. d) The recovery and sorting efficiency value versus different flow rate. e) The recovery ratio of MCF-7 breast-cancer cells spiked into whole blood. f) The recovery ratio of 300 MCF-7 cells spiked into 1, 5 and 10 mL of whole blood aliquots. g) The recovery ratio of 4 selection schemes of 4 breast cancer cell lines spiked into whole blood.

If the transit time for a sorted CTC was shorter than the hydrodynamic switching time, the cell could not be sorted on this platform. The sorting efficiency was thus defined as the number of collected events versus the total number of events that triggered the sorting. Figure 20d shows the values of sorting efficiency at the flow rate of 30 to 100 µL/min. When the flow rate was 30 µL/min, the sorting efficiency was almost 100% because the average transit time at that flow rate was around 10 ms (Figure 20c). This transit time was long enough for the active sorting step to collect the CTCs. The sorting efficiency decreased to 90% at the flow rate of 80 µL/min, and then dropped to 49% when the flow rate was 90 µL/min. Figure 20d also shows the recovery efficiency of eDAR at different flow rates, which had a similar trend compared to the sorting efficiency. However, the recovery efficiency was defined as the number of spiked-in cells versus the number of recovered cells counted using multicolor fluorescence imaging on the eDAR chip. This performance is a combination of many factors, including the antibody-labeling efficiency, the line-confocal detection efficiency and the sorting efficiency. This explains the difference between the recovery and sorting efficiency at the same flow rate. As a result, for this second generation of eDAR, the upper limit of the throughput was 80 µL/min (12.5 min for 1 mL of blood) with an 88% recovery ratio. Although this throughput is higher than most CTC technologies for the analysis of whole blood, it can be further improved by designing a wider blood inlet channel or moving the first detection beam farther up.

Three to 975 MCF-7 cells were spiked into 1 mL of healthy blood to analyze the recovery efficiency at the flow rate of 50 µL/min. The average recovery ratio was 95% with an R^2 value of 0.998 (Figure 20e). Because the concentration of CTCs is usually very low, the enumeration results were affected by the Poisson distribution. In this case, the ability to analyze a larger volume of whole blood sample with an acceptable throughput and recovery ratio was very important. In the first generation of eDAR, the capacity was limited by the number of pores on the polycarbonate filter, which was around 1000. In this reported second-generation eDAR, we had 20,000 mircoslits, which resulted in significantly

increased capacity. We spiked the same number of MCF-7 cells into 1, 5 and 10 mL of healthy blood, and then analyzed these three samples at the flow rate of 50 μL/min. There was no significant change in their recovery ratio (Figure 20f), which shows that our method is capable of running a large amount of whole blood with high efficiency and throughput.

Although EpCAM was used in most of the CTC studies to select tumor cells, increasingly more studies have reported that CTCs with a low EpCAM expression have more mesenchymal characteristics and are more aggressive. The latest eDAR platform is sufficiently flexible to use any labeling scheme to select rare cells so we can capture tumor cells using biomarkers other than EpCAM. We designed three schemes to select different cultured breast cancer cell lines (Figure 20g). EpCAM was used to select MCF-7 cells, Her-2 was used to select SKBr-3 cells, and EGFR was used to select MDA-MB-231 cells. All these three schemes isolated and trapped the targeted cells with a recovery ratio higher than 88%. Another unique and important feature of eDAR is the independence of where the marker is located, such as an intracellular marker like GFP (Figure 19d). The recovery ratio of the MDA-MB-231-GFP cells spiked into whole human blood was 91% (Figure 20g). Since fluorescent proteins are widely used in animal models, such as the HIM model, to study the progression and mechanisms of metastasis, eDAR could be an ideal tool to select CTCs in these models without any immunostaining steps.

In addition to the above technological advancements to translate eDAR for the analysis of patient samples, we have also carried out two sets of experiments to determine: (1) How long will whole blood last if they are to be shipped from Tufts, and (2) Whether we might develop a method for archiving patient samples and preserving the rare cells in blood; this capability will allow us to archive the clinical samples we will collect prospectively (Task 2) so we can return to these samples over time to carry out additional studies.

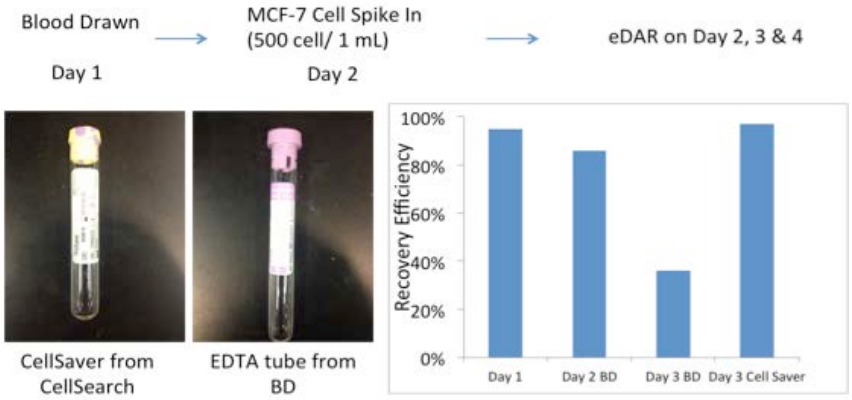

Figure 21. Schematic outlining the experiments we carried out to determine the recovery of spiked-in cancer cells in healthy donor blood after the blood has been stored for 1, 2, 3, and 4 days. We tested two types of tubes, one from BD and one from CellSearch.

Towards answering these two questions, we have mostly completed (1) and determined freshly drawn blood can last for at least three days if stored in the right blood-draw tube, which is sufficient for blood to be shipped overnight to us for analysis. Figure 21 shows our experiment and results, which were performed using spiked-in cultured breast cancer cells. Once we have clinical samples, we will also verify this result with patient samples.

The ability to store whole blood for three days is a critical practical requirement when we begin to analyze clinical samples.

1b. Integrate assays and optical methods developed in Walt lab into a microfluidic device for the analysis and profiling of biomarkers (Years 1-2).

A key step to integrate the single-molecule array technology developed in the Walt lab for the analysis of CTCs is to remove the CTCs from the sample preparation chip described above so that CTCs can be lysed and the important but low abundance protein biomarkers derived from the CTCs can be detected and quantified using the single-molecule array technology. We were able to remove individual CTCs using a micropipette with the first generation eDAR chip. With the second generation eDAR chip, we are also developing a method for the automated second step sorting and dispensing of single cells into an array of microwells for downstream analysis by the digital ELISA technique.

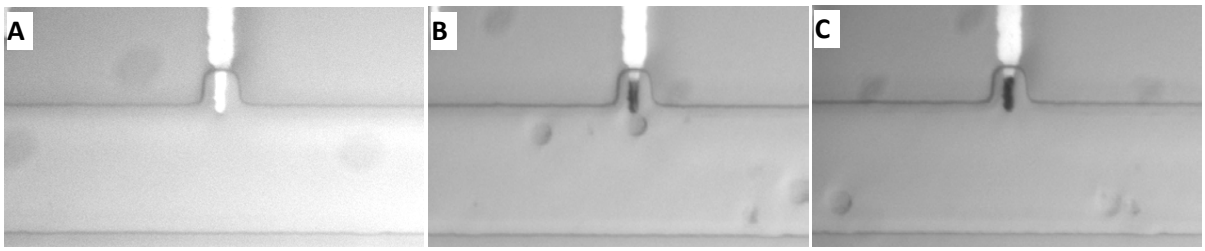

Figure 22. Negative dielectrophoretic capture at BPE anode, followed by release after turning off electric field.

In addition to an automated sorting and dispensing system, the lysing and then mixing of the immuno-magnetic capture beads with the cell lysate is also an important step. Here, we are developing a dielectrophoretic technique that employs bipolar electrodes (BPE) for the parallel trapping, manipulation, and lysis of single cells for downstream analysis using digital ELISA. Figure 22 shows a preliminary experiment where water oxidation led to a charge enrichment region around the BPE tip. A single cell was observed to accelerate towards and then be trapped at the BPE anode (Figure 22B). The cell was trapped at the BPE tip for the remaining duration that the applied field was maintained. After the applied field was turned off, the cell was released as shown in Figure 22C. We discovered that in addition to single-cell trapping and manipulation, we can also employ this method for the controlled lysis of single cells that is needed in the digital ELISA approach to quantitating single-cell protein content.

1c. Develop integrated microfluidic and optical techniques for single cell analysis using model cell lines (Years 1-3).

Another approach to study protein expressions in single cells is with immuno-labeling and fluorescence imaging, which complements the digital ELISA approach that provides higher sensitivity and, more importantly, absolute quantification. We have, therefore, developed a semi-automated system for sequential immunolabeling and photobleaching on the eDAR platform, which allows us to image an arbitrarily large panel of biomarkers, a feat that could not be achieved with traditional formats of immuno-fluorescence imaging. In our experiment, two protein markers of interest, combined with a positive control marker (nuclear stain) and a negative control marker (CD45), are studied in each round. As proof of principle, we performed four rounds of the immunostaining and photobleaching process to look at the expression of eight protein markers of interest.

Overview. We developed an inline staining and washing system coupled with the current eDAR platform in order to minimize the dead volume; decrease the amount of antibodies used; avoid introducing air bubbles; and automate the process. As shown in Figure 23A, two ports on the eDAR microchip were left open to perform the perfusion labeling and washing steps while all the other three ports were completely closed. A peristaltic pump delivered the washing buffer and labeling reagents to the eDAR microchip and was coupled with the pressurized buffer source via a six-way valve. The other three ports on this valve were completely blocked to prevent any possible leakage or contamination. When running the eDAR experiment, the six-way valve was turned to the pressurized buffer side to provide a stable control of the hydrodynamic switching. It was turned to the peristaltic-pump side to inject accurate amounts of reagents to the microchip without introducing any air bubbles. Using this scheme, a few nanograms of the antibodies were introduced to the trapped cells in less than 5 min; a typical incubation step took less than 20 min (Figure 23B).

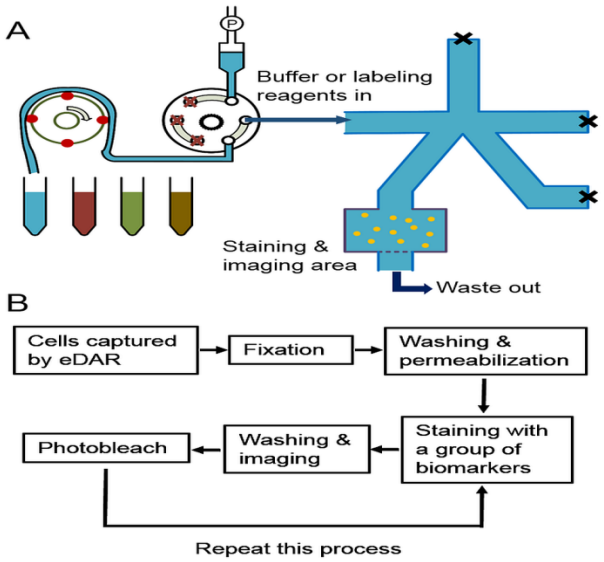

Figure 23. General scheme and procedure of the sequential immunostaining and photobleaching tests. A) The inline labeling system coupled to the current eDAR system. A peristaltic pump delivered the labeling reagents and washing buffer. The cross bars on this figure mean the corresponding ports were closed during the experiments. B) The general process flow of the sequential immunolabeling and photobleaching experiment.

Characterization and optimization of the photobleaching process. There are two critical factors that could determine the efficiency of the photobleaching step—exposure power and time. We carefully characterized and optimized them to improve the efficiency and throughput while ensuring that the cells were not damaged by potential heating. The photobleaching curve under different exposure powers was studied first (Figure 24A). MCF-7 breast cancer cells were labeled with anti-EpCAM-PE, and placed on a No.2 coverslip. We bleached the labeled single cells with three different power settings. The bleaching curves show that the exposure time could be controlled under 10 min to get a more than 95% bleaching efficiency when the exposure power was higher than 2 mW.

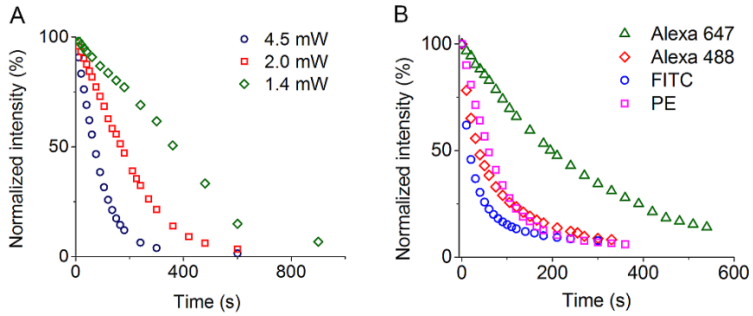

Figure 24. (A) Photobleaching curves for the MCF-7 cells labeled with anti-EpCAM-PE exposed to different powers of the light source. (B) Photobleaching curves for the MCF-7 cells labeled with anti-EpCAM conjugated with Alexa 647, Alexa488, FITC and PE.

Based on this result, we studied the bleaching curves of the four fluorophores, PE, FITC, Alexa 488 and Alexa 647, which could be directly applied in our scheme. Figure 24B shows that the fluorescent emission of PE, FITC and Alexa 488 could be bleached to less than 10% in less than 5 min; the photobleaching times for Alexa 647 took longer, partly because the power of the light source between 610 to 660 nm (red excitation) was lower than that in the range of yellow and green excitation. As a result, we set the bleaching time at 15 min to get a high bleaching efficiency with an acceptable throughput. This time could be improved by raising the power of the light source; however, it might increase the risk of heating and cellular damage.

Sequential immunostaining and photobleaching tests. For this part of the study, we designed an assay for the expression of protein markers on captured CTCs based on four rounds of sequential immunostaining and photobleaching processes. We monitored four different markers in each round through four individual channels using epi-fluorenscence microscopy. Each set of markers had a nuclear stain (Hoechst) as a positive control marker, CD45 conjugated with FITC as a negative control marker, and two protein markers conjugated with PE or Alexa 647. Our system was designed not to bleach the Hoechst stain for two reasons: First, because the stain was used as a positive control marker, we could not keep track of it if we photobleached it. Second, it would require a UV exposure to bleach the stain,

which could cause significant cellular damage. CD45 is widely expressed on many types of white blood cells (WBCs), which are considered to be the biggest interferences in the separation of CTCs. Therefore, they are frequently used as negative control markers.

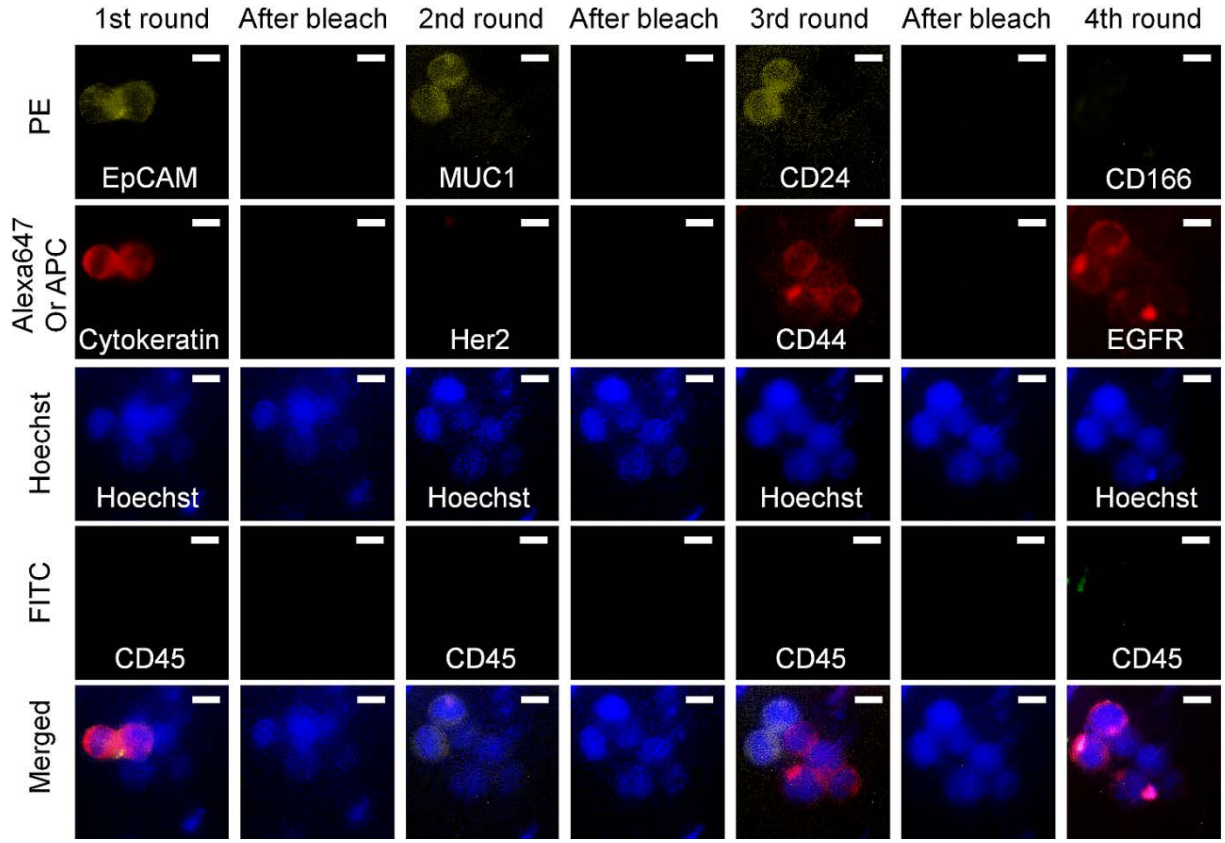

Figure 25. Sequential immunostaining and photobleaching results for six cancer cells trapped on an eDAR chip. The Hoechst nuclear stain was used as a positive control marker and CD45 was used to exclude the potential interference from WBCs. Eight protein markers were studied, including EpCAM/Cytokeratin, MUC1/Her2, CD44/CD24 and CD166/EGFR.

Many protein markers could be tested on CTCs but as a proof of concept, we selected eight antigens and divided them into four groups (Figure 25). The first set had EpCAM and cytokeratin, which are the most widely used markers to identify CTCs. We applied this immunostaining test set right after the capture of CTCs by eDAR to further confirm and enumerate the CTCs with epithelial biomarkers. Figure 25 shows that there were six tumor cells trapped on the eDAR chip, which are positive to the Hoechst stain but negative to CD45. Two of them had a strong expression of EpCAM and cytokeratin, which implied the cells had epithelial characteristics.

The second set was designed to investigate other epithelial markers which are important for clinical and biological studies. We selected Her2 and MUC1 as the two protein markers for this set since these two biomarkers play important roles in the cancer pathogenesis and resistance to drugs. They are also potential targets of the anti-tumor drugs and immunotherapy. The second round of labeling in Figure 25 shows that part of the cells trapped on the eDAR-chip had MUC1 expression but all of them were really low in their Her2 expression. However, in other experiments, we did observe cells expressing Her2 strongly.

Cancer stem cells have been shown to play important roles in tumor progression and have been observed in the population of CTCs. The third set of markers had two cancer stem cell antigens, CD44 and CD24. They are extensively studied as stem cell markers for breast cancer and possibly for other

types of cancers as well. The data in figure 25 shows that four cells had a strong expression of CD44+/CD24-, and the other two are CD44-/CD24+. Other stem cell markers, such as CD133 and CD105, could also be used in this group based on the type of primary cancer.

The last set of markers in Figure 4 was designed to look at the expression of EGFR and CD166 to demonstrate the mesenchymal characteristics of tumor cells. EGFR has been shown to be associated with the EMT process, and CD166 was used to define mesenchymal stem cells in bone marrow. Other related markers, such as vimentin and cadherin, could be used in this group as well.

This downstream immuno-fluorescence imaging method is a complementary part of eDAR and digital ELISA in the future to benefit studies of CTC subpopulations and quantitatively monitor the expression of multiple CTC protein biomarkers. To facilitate the detection and imaging of CTCs, we have also developed a fluorinated fluorescent nanoparticle probe that performs better than conventional dyes in cell labeling brightness.

Task 2. Work with the Walt lab to apply these methods to breast-cancer patient samples for the detection and validation of protein and cell biomarkers *(Months 25-60).*

2a. Develop/submit amended proposal to University of Washington IRB to permit secondary use of currently archived patient samples (Months 1-12).

This task has been completed per last year's annual report.

2b. Apply sensitive techniques (1a and 1b) for the retrospective analysis and validation of biomarkers from archived patient samples (Months 25-60).

We propose to use archived blood plasma samples from breast cancer patients. One hundred archived blood plasma samples already exist in the Chiu lab from a previous three-year study on detection of biomarkers in breast cancer patients. But these studies have not been initiated per SOW.

2c. Apply sensitive techniques (1a and 1b) for the prospective analysis and validation of biomarkers from patient samples (Months 36-60).

These studies have not been initiated per SOW.

2d. Apply techniques developed for the prospective analysis of cancer cells (1a and 1c) from patient samples obtained in 2c with single-cell resolution (Months 36-60).

These studies have not been initiated per SOW.

Charlotte Kuperwasser, PhD, Tufts University School of Medicine, 750 Washington St., Box 5609, Boston MA 02111

Task 1. Early Detection (Months 1 to 36)

1a. Utilize the 'Human-In-Mouse' breast tumor model to determine if one can identify biomarkers of early tumor progression and tumor growth. Collect blood and breast tissues at various stages of progression: Normal, hyperplasia, DCIS, invasive cancer (Months 1-18). HIM tumors will be creased from human breast epithelial cells collected from discarded tissues of women who have undergone reduction mammoplasty surgeries. For more information/details on model: Nature Protocols, 2006, 1, 595-599.

As described above, we generated orthotopic humanized tissue-transgenic breast cancers using mammary epithelial cells obtained from reduction mammoplasty tissues from patients undergoing elective surgery. In order to examine earlier stages of tumor development including DCIS and hyperplasia, we have generated HIM tumors using SV40er/Ras transgenes, as this approach models tumor progression in a well-defined manner. We have collected blood for the purpose of assessing single

molecular diagnostic potential at these early time points in tumor progression and have provided these samples to the Walt Laboratory for analysis. We have also expanded the HIM tumors utilized in these studies to include additional mutations, such as PI3K E545K and PI3K H1047R, MAGI3:Akt3, and mutations in TBX3. This list will continue to expand as we revise the biomarker list.

1b. Utilize the 'Human-In-Mouse' breast tumor model and inject different cancer to normal cell ratios—1:10, 1:100, 1:1000 (Months 18-32).
Predicted Total mice=(80x2 replicates)=160; Predicted total number of reduction mammoplasty tissues=10.
These studies have been initiated and will continue over the next year per SOW.

Task 2. Response to chemotherapy and hormone therapy (Months 24-48).

2a. Inject traditional breast cancer cell-line based xenografts into mice using hormone receptor positive lines and hormone receptor negative and Her2+ lines (MCF7, T47D, HCC1418, SUM225, BT20, SUM149, SUM159)(Months 24-36). Human breast cancer cell lines are all commercially available and previously characterized. For more information/details on these cell line-based xenografts see: Breast Cancer Research, 2010;12(5):1-17.

Cell-line based xenografts have been initiated and terminal blood collections have been made with MCF7, T47D, BT20, and SUM1315 lines. Chemotherapy and hormone therapy treatments and studies have not yet been initiated.

2b. Allow tumors to form and reach 5mm and assess serum levels of EMT/SCS markers. (Months 24-36).

These studies have not yet been initiated per SOW.

2c. Treat animals with chemotherapy (Paclitaxel/Taxol) or anti-estrogen (Tamoxifen) and measure serum levels of EMT/CSC markers and mtDNAs during tumor regression and after cessation of therapy. (Months 24-48).

These studies have not yet been initiated per SOW.

2d. Continue to monitor tumor growth. (Months 36-48).

These studies have not yet been initiated per SOW.

2e. Determine whether the levels of EMT/CSC markers correlate to response to therapy or to tumor recurrence (Months 36-48).
Predicted Total Mice=(30x2 replicates)=60.

These studies have not yet been initiated per SOW.

Task 3. Recurrance prediction (Months 36-60).

These studies have not yet been initiated per SOW.

3a. Create tumors using the 'Human-In-Mouse' breast tumor model. Allow tumors to form and reach 5-8mm in diameter and assess serum levels of oncogenes used to create tumors (Months 36-50).

These studies have not yet been initiated per SOW.

3b. Surgically resect the tumors and measure blood serum levels of EMT/CSC markers as well as mitochondrial DNAs during tumor regression and after cessation of therapy after surgery (Months 36-50).

These studies have not yet been initiated per SOW.

3c. Monitor mice and measure the levels of EMT/CSC markers weekly to determine if they increase or correlate with regrowth of tumor (Months 48-60).
Predicted Total Mice=(80x2 replicates)=160; Predicted total number of reduction mammoplasty tissues=10.
These studies have not yet been initiated per SOW.

Gail E. Sonenshein, Ph.D., *Tufts University School of Medicine 150 Harrison Avenue Boston, MA 02111*

Task 1. Perform mitochondrial DNA mutational analysis. (Months 1 to 16).

1a. Isolate mitochondria from cultured mouse and human mammary breast epithelial or cancer cells that exist in our laboratory and extract DNA and subject it to massively parallel sequencing and bioinformatics to identify mutations. (Months 1-8).
As mentioned in our previous progress report, we have developed the technologies and used them to characterize the mitochondrial DNA sequences in human and mouse cell lines and tumor tissue. **Thus this task is essentially completed. However, as new inflammatory breast cancer (IBC) cell lines are established or as we acquire additional lines, we are analyzing their mtDNA sequences to increase our database.** To this end, we have extended our previous analysis of mtDNA mutations in ER -cell lines to MDA-MB-468 and inflammatory breast cancer (IBC) lines to a newly developed primary IBC cell line—MDA-IBC-3 kindly provided by Wendy Woodward (MD Anderson) (**Table 2**). The MDA-IBC-3 cell line was generated from primary human breast cancer cells isolated from the pleural effusion of a patient with IBC.

Untransformed	**ER**	**ER -ve**	**Inflammatory breast cancer (IBC)**	**Carcinogen treated**
HMEC	MCF7	BT549	SUM149	BP1
MCF10A	T47D	MDA-MB-231	SUM190	D3
		Hs578T	**MDA-IBC-3**	
		MDA-MB-468		

Table 2: Table listing the panel of untransformed breast epithelial and breast cancer cell lines from which mitochondrial DNA was isolated and analyzed. The analyses of MDA-MB-468 and MDA-IBC-3 cell mtDNA represent updated data.

1b. Isolate mitochondria from normal tissue and from tumors, extract DNA and subject it to massively parallel sequencing (Months 8-12).
To set the stage for analysis of tumor tissue, we have obtained mouse tumors derived by injection of stem-like SUM149 IBC cells in an orthotopic model. We have isolated mtDNA from the tumor tissue and compared the DNA sequence to that of the parental SUM149 cell line. We could detect all mutations observed in parental SUM149 cells in the tumor tissues. Interestingly, no new mutations were seen. In a second experiment, we isolated and sequenced mtDNA from tumors derived from MDA-MB-231 cells. We similarly found that the mtDNA sequence in the tumor tissue and cell lines was identical. These results confirm that we can identify mtDNA mutations in tumor samples obtained from mice and are ready to analyze tumor tissue obtained from the HIM breast tumor model, which will be provided by the Kuperwasser lab (Task 3a).

1c. Compare mtDNA from normal mouse mammary tissue and from tumor tissue using bioinformatics to identify mutations. (Months 10-16).

We have isolated mtDNA from a MMTV-c-Rel mouse mammary parental line and from a derivative of this line following transformation by DMBA. The analysis of mouse mtDNA required the development of new mouse mtDNA specific primers, which were designed based on those of Tanhauser and Laipis[12], and have been successfully tested. However, we are finding that the DNA fragments are too large to be sequenced fully in our facility. Thus, we are in the process of testing new primers. Once identified, the isolated mouse mtDNA will be sequenced with these new mouse specific primers.

Task 2. Characterize mtDNA mutations resulting from oncogene expression in murine breast tumors (Months 16-24).

We have now collected blood samples at various time points from mice carrying tumors of various sizes derived from MDA-MB-231 cells to test the sensitivity of the isolation and amplification procedures when tumor burden is low. These analyses are currently in progress. We have also recently developed a method to isolate mtDNA from formalin fixed paraffin embedded (mouse) tissue. As the DNA from these samples was relatively small, we designed new primers that amplify smaller pieces of DNA. Using the DNA encoding all tRNAs, which have been associated with a significant number of genetic disorders, as our region of choice, we have optimized a protocol that allows for specific amplification of the regions encoding all of the 22 tRNA's present in the mtDNA. The 22 tRNA primer sequences were obtained from Grzybowska-Szatkowska et al.[13] (**Table 3**). We used these primers to confirm the tRNA mutations we observed in IBC cell lines SUM149 and SUM190 (**Table 4**). We propose to test whether these primers can be used to detect and quantify breast metastases, e.g., to the brain or lungs of mice.

Gene	Product	Gene position in mtDNA (bp) AC_000021	Primer position (bp)	Primer sequence 5′–3′
TRNF	tRNA-Phe	577–647	510–526	CCAGCACACACACACCG
			1703–1720	GCTAAGGTTGTCTGGTAG
TRNV	tRNA-Val	1602–1670	510–526	CCAGCACACACACACCG
			1703–1720	GCTAAGGTTGTCTGGTAG
TRNL1	tRNA-Leu	3230–3304	3170–3190	CCCGTAAATGATATCATCTCA
			4190–4207	CACTCACCCTAGCATTAC
TRNI	tRNA-Ile	4263–4331	4190–4207	CACTCACCCTAGCATTAC
			4531–4549	AATCAGTGCGAGCTTAGCG
TRNQ	tRNA-Gln	4329–4400	4190–4207	CACTCACCCTAGCATTAC
			4531–4549	AATCAGTGCGAGCTTAGCG
TRNM	tRNA-Met	4402–4469	4190–4207	CACTCACCCTAGCATTAC
			4531–4549	AATCAGTGCGAGCTTAGCG
TRNW	tRNA-Trp	5512–5579	5428–5444	CAAAACCCACCCCATTC
			5943–5966	TAATAGGTATAGTGTTCCAATGTC
TRNA	tRNA-Ala	5587–5655	5428–5444	CAAAACCCACCCCATTC
			5943–5966	TAATAGGTATAGTGTTCCAATGTC
TRNN	tRNA-Asn	5657–5729	5428–5444	CAAAACCCACCCCATTC
			5943–5966	TAATAGGTATAGTGTTCCAATGTC
TRNC	tRNA-Cys	5761–5826	5428–5444	CAAAACCCACCCCATTC
			5943–5966	TAATAGGTATAGTGTTCCAATGTC
TRNY	tRNA-Tyr	5826–5891	5428–5444	CAAAACCCACCCCATTC
			5943–5966	TAATAGGTATAGTGTTCCAATGTC
TRNS1	tRNA-Ser	7446–7514	7374–7393	AACCTGGAGTGACTATATGG
			7744–7790	GCAGGATAGTTCAGACG
TRND	tRNA-Asp	7518–7585	7374–7393	AACCTGGAGTGACTATATGG
			7744–7790	GCAGGATAGTTCAGACG
TRNK	tRNA-Lys	8295–8364	7744–7790	GCAGGATAGTTCAGACG
			8635–8656	TGATTAGTCGGTTGTTGATGAG
TRNG	tRNA-Gly	9991–10058	9917–9935	CGCCGCCTGATACTGGCAT
			10511–10530	CTAGTATTCCTAGAAGTGAG
TRNR	tRNA-Arg	10405–10469	9917–9935	CGCCGCCTGATACTGGCAT
			10511–10530	CTAGTATTCCTAGAAGTGAG
TRNH	tRNA-His	12138–12206	12059–12079	AACACCCTCATGTTCATACAC
			12525–12544	TGGCTCAGTGTCAGTTCGAG
TRNS2	tRNA-Ser2	12207–12265	12059–12079	AACACCCTCATGTTCATACAC
			12525–12544	TGGCTCAGTGTCAGTTCGAG
TRNL2	tRNA-Leu2	12266–12336	12059–12079	AACACCCTCATGTTCATACAC
			12525–12544	TGGCTCAGTGTCAGTTCGAG
TRNE	tRNA-Glu	14674–14742	14051–14073	CCACCTCCATCATCACCTCAAC
			14716–14743	GTTCTTGTAGTTGAAATACAACGATGG
TRNT	tRNA-Thr	15888–15953	15583–15605	AATTCTCCGATCCGTCCCTAAC
			16097–16118	ATGGTGGCTGGCAGTAATGTA
TRNP	tRNA-Pro	15956–16023	15583–15605	AATTCTCCGATCCGTCCCTAAC
			16097–16118	ATGGTGGCTGGCAGTAATGTA

Table 3: The table depicts the primer sequences used to amplify the 22 tRNAs using PCR

Cell lines	SUM149	SUM190
mtDNA mutation	7521 G>A tRNA-Asp	10005 A>T tRNA-Gly

Table 4: tRNA mutations were confirmed using the 22 tRNA primers in SUM149 and SUM190 cell lines

2a. Compare mtDNA from mammary tissue vs tumors or derived cell lines of transgenic mice driven by oncogenes implicated in breast cancer. Samples obtained from Kuperwasser (months 16-24)
These studies are awaiting development of primers for full amplification of the mouse mtDNA. The sequencing should be initiated shortly.

2b. Characterize mtDNA alterations in tumor lines that will be utilized by the Kuperwasser laboratory in their 'HIM' analysis. DNA samples will be analyzed as in Task 1 above (Months 18-24).
The Kuperwasser laboratory has proposed using ERα+ tumor lines MCF7 and T47D and we have finished characterizing mtDNA alterations in these lines. Our data are summarized in **Table 5** below. We are thus prepared to perform mtDNA sequence analysis to compare mammary tissue with tumor tissue derived from the HIM tumors to be provided by the Kuperwasser lab.

MCF7		**T47D**	
263	**A>G**	**263**	**A>G**
315	**INS C**	309	INS C
750	A>G	**315**	**INS C**
1438	**A>G**	**1438**	**A>G**
2591	A>G	2355	A>G
4769	**A>G**	2442	T>C
5899	INS C	2706	A>G
6776	T>C	3847	T>C
8860	**A>G**	4767	A>G
9966	G>A	**4769**	**A>G**
13260	T>C	7028	C>T
14319	T>C	**8860**	**A>G**
15326	**A>G**	13188	C>T
15380	A>G	13481	G>A
16148	C>T	14766	C>T
16519	**T>C**	**15326**	**A>G**
		15674	T>C
		16362	T>C
		16519	**T>C**

Table 5: Table showing the mtDNA mutations observed in MCF and T47D cell lines. **Bold** font indicates the mutations found in common between the two cell lines

Task 3. Recurrence prediction: Determine whether mtDNA mutations can be used to test for breast tumor regression in mice (in collaboration with Kuperwasser) (Months 18-60).

3a. mt DNA from tumor samples provided by the Kuperwasser laboratory using the HIM breast tumor model. Tumors will be initially removed after they have been allowed to reach 5-8 mm in diameter and then at the end of the experiment (Months 18-30)
As discussed above, we have developed the technology for these studies, and have very recently initiated them.

3b. DNA will be isolated from serum collected before resection and weekly after resection that will be provided by the Kuperwasser laboratory (Months 18-30).

As a prerequisite for analysis of serum, we needed to be able to amplify mtDNA from whole blood of mice bearing a human tumor. To develop this technique, blood from mice containing MDA-MB-231 cell-derived tumors of ~1 cm^3 was analyzed. We were able to isolate total DNA from whole blood obtained from mice; whereas, almost negligible amounts of DNA were isolated from plasma. The DNA from the whole blood was subjected to the PCR protocol described above, but our initial analysis showed multiple additional bands. Thus we sought to improve the fidelity of the PCR process and tested several high fidelity polymerases. We observed that the New England Biolabs Q5 High Fidelity polymerase successfully amplified the DNA and gave reproducible, specific bands as seen with the amplified DNA from the whole blood of mice (**Figure 26**). Thus, we will use the Q5 polymerase in future analyses.

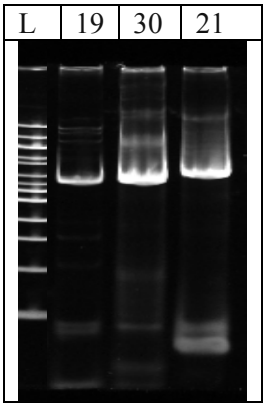

Figure 26: Acrylamide gel showing PCR product obtained after amplification of total DNA obtained from mouse blood using Q5 polymerase.

We are currently in the process of testing the sensitivity of the isolation and amplification procedures using mice bearing tumors of various sizes derived from MDA-MB-231 cells. Specifically, mice were bled when the tumors were only beginning to be palpable to verify our ability to isolate and detect mtDNA when tumor burden is low. The DNA is currently being analyzed.

In summary, essentially all of the technology needed to isolate, amplify and analyze mtDNA from tumor tissue and from blood has now been developed in our laboratory. Thus, during the next year, we will be working closely with the Kuperwasser group to analyze mtDNA in early stages of tumor progression, such as DCIS and hyperplasia, as well as in advanced tumors with metastasis.

Task 4. New Task.

As discussed above, miRNA represent potential biomarkers for breast cancer detection as some are released from tumor cells and can be present stably in the blood stream. As described previously, we are also identifying miRNAs regulated by ADAM8, which was not part of the original SOW, in order to elucidate new important breast cancer biomarkers for the Walt Lab to develop a detection assay. We have demonstrated that ADAM8 (**a d**isintegrin **a**nd **m**etalloprotease protein 8) is a key downstream mediator of a RelB NF-κB pathway that promotes a more aggressive phenotype of breast cancer. ADAM8 belongs to a disintegrin and metalloprotease (ADAM) protein family, which mediate cell adhesion, migration, signaling and proteolysis of extracellular matrix. To date, we have shown that *ADAM8* is overexpressed in breast tumor samples *vs* normal breast tissue, especially in ER-negative and triple-negative breast cancers. Interestingly, *ADAM8* mRNA levels correlate with metastatic relapse in patients. Using immunohistochemistry, our collaborators in France have shown that 34% of triple negative tumors and 48.2% of breast metastases are positive for ADAM8 staining. *In vivo*, ADAM8 knockdown strikingly

prevented tumor development and spreading of circulating tumor cells from MDA-MB-231 cells in an orthotopic mammary mouse model and metastases to the brain, bone, liver and lungs following cardiac injection. Consistently, ADAM8 plays an essential role in breast cancer cell migration, invasive outgrowth and anchorage-independent growth.

Buchsbaum Laboratory—Tufts Medical Center

Section 1

The research effort includes both laboratory and clinical research aims. The purpose of the laboratory effort is to determine the effect of the tumor microenvironment on serum markers of metastasis in the HIM model. The purpose of the clinical research effort is to validate the serum markers of metastasis derived from the Walt and Chui pre-clinical experiments using human serum samples.

Section II

Task 1. Determine effect of tumor microenvironment on serum markers of metastasis in the HIM model (Months 1-36).
1a. Develop mammary fibroblast lines with range of Tiam1 (both down- and up-regulated). (Months 1-6)
This task has been completed. As reported previously, we have generated mammary fibroblasts with stable silencing of Tiam1 expression, stable over-expression of Tiam1, and corresponding control lines. We have tested these lines in our 3D co-culture model to verify the effect on co-cultured mammary tumor cell lines in terms of migration, invasion, and modulation of cancer stem-cell like populations. We have found that altering Tiam1 expression in mammary fibroblasts leads to converse changes in cancer cell invasion and migration, as shown below:

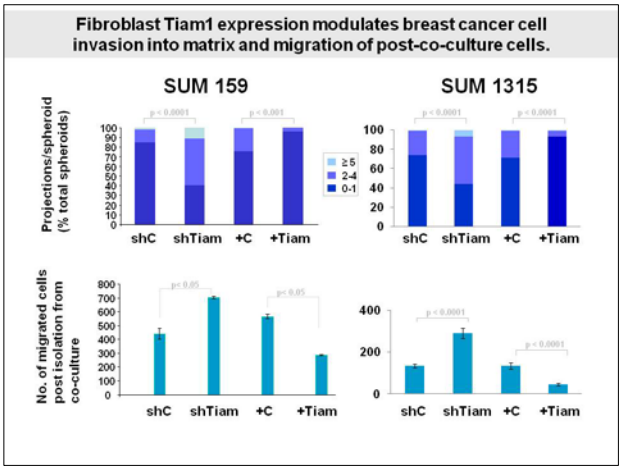

Figure 27: Fibroblast Tiam1 expression modulates breast cancer cell invasion into matrix and migration of post-co-culture cells.
Top panels: Number of projections/spheroid for indicated pairs of breast cancer cell lines and mammary fibroblasts in 3D mixed cell spheroid co-culture.
Bottom panels: Transwell migration of breast cancer cells isolated from 3D mixed cell spheroid co-culture with indicated mammary fibroblasts. C = control; sh = silencing hairpin pSuperior vector; + = pBabe over-expression vector.

We have also found that altering Tiam1 expression in mammary fibroblasts leads to converse changes in cancer stem-cell like populations, as measured by tumorsphere assays, flow cytometry, and serial dilution primary implantation and serial passage in the HIM model, as shown below:

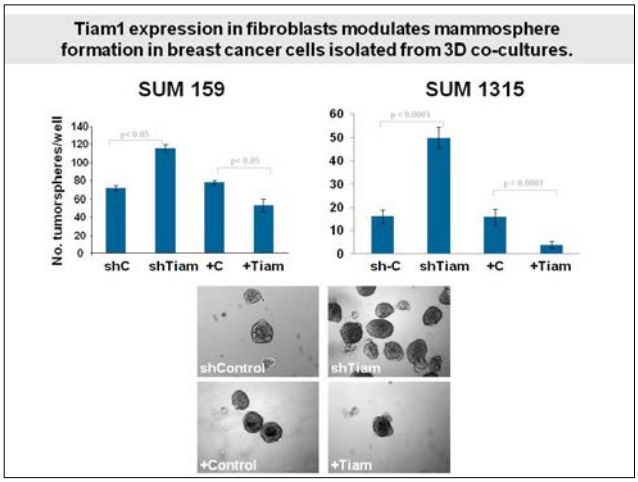

Figure 28: Tiam1 in fibroblasts modulates tumorsphere formation in breast cancer cells isolated from 3D co-cultures.
Top panels: Breast cancer cells isolated from 3D co-culture with indicated mammary fibroblasts were cultured at low density under ultra-low adherence conditions and the number of tumorspheres was quantitated under light microscopy.
Bottom panels: representative light microscope images of tumorspheres.

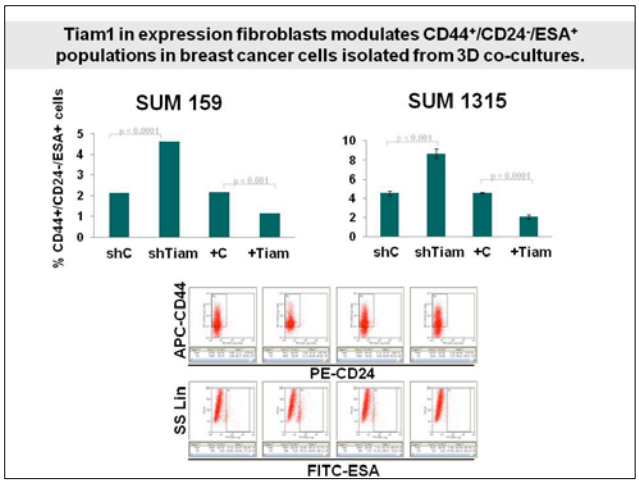

Figure 29: Fibroblast Tiam1 expression modulates $CD44^{+}/CD24^{-}/ESA^{+}$ populations in breast cancer cells isolated from 3D co-cultures.
Populations of breast cancer cells were analyzed by flow cytometry for expression of indicated cell surface markers using fluorophore-conjugated antibodies after isolation from 3D co-culture with indicated fibroblasts.
Top panels: quantification of duplicate experiments, each done in triplicate.
Bottom panels: representative flow cytometry results.

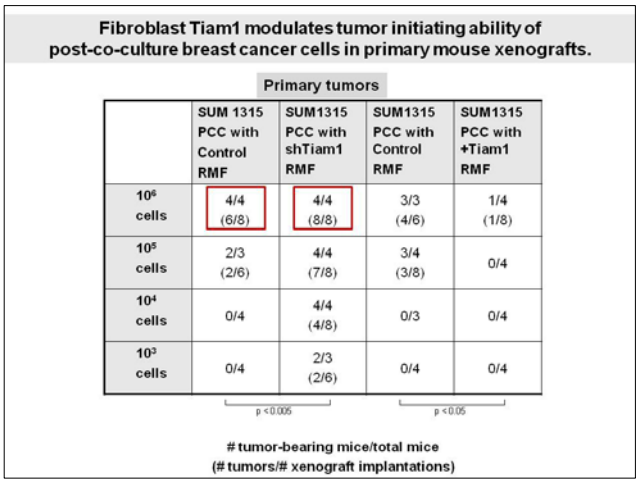

Figure 29: Fibroblast Tiam1 modulates tumor initiating ability of post-co-culture breast cancer cells in primary mouse xenograft model.
Breast cancer cells isolated from 3D co-culture with indicated mammary fibroblasts were implanted in Matrigel plugs into mouse mammary fat pads in serial dilution. Cancer cells isolated from 3D co-culture with Tiam1-deficient fibroblasts had increased tumor initiation in the HIM model compared with controls. Cancer cells isolated from 3D co-culture with Tiam1-over-expressing fibroblasts had decreased tumor initiation in the HIM model compared with controls. Size-matched tumors (red boxes) were used in serial implantation in secondary recipients (**Figure 30**).

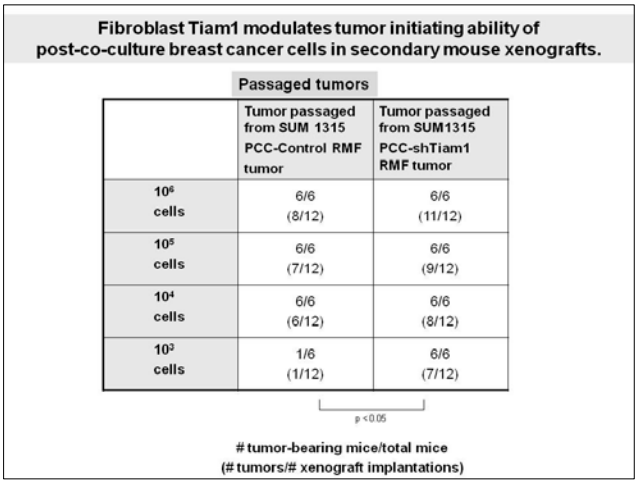

Figure 30: Fibroblast Tiam1 modulates tumor initiating ability of post-co-culture breast cancer cells in secondary recipients of passaged tumors.
Primary tumors of equivalent size were harvested from tumor-bearing mice (indicated by red boxes in preceding figure), digested to single cell suspensions using mechanical means combined with a collagenase-trypsin-DNAse protocol, and passaged into mammary fat pads of secondary recipients in serial dilution as indicated. Primary tumors arising from cancer cells isolated from 3D co-cultures with Tiam1-deficient fibroblasts had increased tumor initiation in secondary recipients.

Results of these in vitro experiments were correlated with metastasis in the HIM model, as detailed below.

1b. Utilize HIM breast tumor model in collaboration with Dr. Kuperwasser. Allow tumors to reach 10mm in diameter. Monitor mice weekly and assess serum levels of biomarkers of early tumor progression and tumor growth using single molecule diagnostic assays developed in Walt lab (see Walt task 1; Months 6-18). Numbers of mice needed = 10 different experimental conditions x 20 mice per experimental cohort = 200 mice.

We have now established two models of human breast cancer metastasis in mice, based on the HIM model and a modification (detailed below). Xenografts have been established in 128 total mice to date. Serum samples were collected biweekly rather than weekly, due to frailty of the mice after tumor implantation, and terminal serum samples were obtained at sacrifice. All serum samples have been frozen. All mice have been sacrificed. Pathologic analysis has been completed on tumors and lung samples from all mice.

Model 1 of human breast cancer metastasis. We have established tumor cell implantation in the original HIM model in 112 mice to date (primary implantations in 64 mice and secondary passage in 48 mice). We have found that the secondary passage protocol is an excellent model of breast cancer metastasis to lung that can be manipulated by altering the cancer-associated fibroblasts in the model. This protocol involves exposing SUM1315 human breast cancer cells to mammary fibroblasts in three-dimensional spheroid co-cultures, isolating the cancer cells and establishing xenografts in mice, and then passaging the xenografts to secondary recipients. In the cohort of 48 mice established according to this protocol, mice developed a high burden of lung metastases relatively quickly (22 of 24 mice with >10 mets, the remaining two mice with 5-10 mets; time frame = ≤ 4 weeks) after implantation with passaged xenografts arising from SUM1315 breast cancer cells exposed to Tiam1-deficient fibroblasts, based on histology of fixed tissues post-necropsy. In contrast, control mice developed significantly fewer tumors and had significantly less metastatic burden (only 5 of 24 mice with 5-10 mets, none with >10 mets).

These results, in combination with the in vitro studies above, indicate that we have established a reliable method for modulating human breast cancer metastasis in the HIM model, and that we can use our in vitro assays to predict conditions that correlate with in vivo metastasis.

Model 2 of human breast cancer metastasis. We have also developed a second model of breast cancer metastasis to lung in a modification of the HIM model. In this protocol, 3D co-cultures are established with breast cancer cells and mammary fibroblasts as above, and when cultures are mature the cancer cells are isolated from the 3D cultures, purified by FACS and then implanted into the mice. We have performed this protocol in 16 mice to date, using co-cultures established with control or Tiam1-deficient

fibroblasts, in the absence or presence of a chemical inhibitor to the Tiam1 deficiency pathway (4 cohorts of 4 mice each). The burden of lung metastases in these mice is tabulated below in Table 6 (low = 1-4 mets; moderate = 5-9 mets; high = ≥ 10 mets):

Table 6

Control fibroblasts	**Control fibroblasts + inhibitor**	**Tiam1-deficient fibroblasts**	**Tiamb1-deficient Fibroblasts + inhibitor**
Moderate	None	High	None
Low	None	High	None
Low	None	High	None
Low	None	High	None

Thus we have established a second reliable model of human breast cancer metastasis in mice. Serum samples have also been collected and stored from this cohort. Both models can be used for generation of serum samples for testing for serum markers of metastasis, and present more reliable methods for controlling metastatic burden as compared to primary tumor implantation alone without fibroblast manipulation.

Task 2. Perform retrospective clinical trial to validate candidate markers from Walt single molecule studies using banked repository samples. (Months 1-60)
This task is largely on hold until candidate markers have been identified and validated using the Walt single molecule studies, as successful application to access banked samples from current repositories will require supporting pre-clinical data. Similarly, determining sample size will be most accurately done once the sensitivity and specificity of the assay for the specific candidate marker(s) has been determined.

2a. Work with statisticians to determine needed sample size for retrospective trial (Months 1-3).
2b. Identify study populations with available serum samples and adequate duration of follow-up to permit retrospective studies (e.g. Nurses Health Study, NCI repositories, or commercial sources such as Bioserve Human Serum Repository) (Months 3-6).
2c. Develop/submit research proposals and regulatory documents to obtain sample access (Months 6-12).
2d. Develop/submit proposal to IRB for retrospective study of de-identified samples (Months 12-18).
These studies have not yet been initiated per SOW.

2e. Obtain samples from subjects for analysis of serum markers identified through the HIM model studies (Months 18-24).
These studies have not yet been initiated per SOW.

2f. analyze results of candidate marker screening of banked samples with regard to correlation with clinical outcomes (Months 30-60).
These studies have not yet been initiated per SOW.

Task 3. Perform prospective clinical trial for predictive and prognostic markers in women with newly diagnosed breast cancer (Months 1-60).
Progress on developing a bank of human serum samples for validation of candidate markers is continuing. The goal is to bank serum samples from all women with newly diagnosed breast cancer, women who are being followed after completing treatment for localized breast cancer, and women with active metastatic breast cancer being treated at Tufts Medical Center. The plan involves coordination of the multi-disciplinary services involved in the care of these patients, and collection and storage of samples under the aegis of the Tufts Medical Center Cancer Center Tissue Repository. At this time the regulatory steps

have been completed and the process of collecting blood samples from eligible patients with history of breast cancer and/or metastatic disease is now underway. Logistics enabling collection of samples from women with newly diagnosed breast cancer prior to treatment are still in process. We are still in the process of operationalizing the best way to obtain appropriate consent for tissue banking for patients with newly diagnosed disease who have not yet undergone surgery. This has been delayed both by the multiple parties involved in decision-making around OR processes and recent changes in leadership within the Tufts Cancer Center.

3a. Work with statisticians to determine needed sample size for prospective trial (Months 1-3).
The number of human subject samples will be determined based on the sensitivity of the assay we develop and the number of markers to be tested, once validated in the HIM model.

3b. Develop and submit proposal to IRB for prospective study of serum samples for tumor markers from women with newly diagnosed breast cancer (Months 1-12).

3b. Coordinate with affiliate institutions to open multi-center trial to facilitate enrollment (Months 1-12).

3c. Enroll patients and gather serum samples: at diagnosis, post-treatment, and every 6 months after treatment for 5 years (Months 12-60 and then ongoing).

3d. Monitor for breast cancer recurrence and metastasis and correlate with levels of serum tumor markers (Months 12-60 and then ongoing).

3e. Collaborate with statisticians on data analysis at interim time points (Months 12-60 and then ongoing).

3f. Monitor for breast cancer recurrence and metastasis and correlate with levels of serum tumor markers (Months 12-60 and then ongoing).
3g. Collaborate with statisticians on data analysis at interim time points (Months 12-60 and then ongoing).

Task 4. Obtain clinical tumor samples for single cell analysis to determine tumor composition (see Walt task 3) and analysis of mtDNA (see Sonenshein task 4). (Months 1-60)
These studies have not yet been initiated per SOW.
4a. Work with breast surgeons and pathologists at Tufts Medical Center to develop technique for harvesting cells in fluid phase from fine needle aspirate (FNA) samples from murine tumors in HIM model (Months 1-12).
4b. Develop and submit proposal to IRB for collection and prospective study of newly collected breast cells obtained from human subjects via FNA as in task 4a; submit regulatory documentation to DOD (months 12-24).
4c. Recruit human subjects, obtain samples, and provide to Walt lab for single cell analysis studies (Months 25-36).
This study will initially be proposed as a pilot study of samples from 20 non-cancer and 20 breast cancer subjects, numbers that can practicably be obtained within a 12 month period.
4d. Work with statisticians to revise number of subjects needed based on initial results of single cell analysis and mtDNA analysis (see Walt Task 3d and Sonenshein Task 4b; months 25-36).
4e. Submit amended IRB proposal adjusting sample size as per 4d (Months 36-42).
4f. Recruit subjects, obtain samples, and provide to Walt lab for single cell analysis studies and to Sonenshein for mtDNA studies (Months 42-60).

KEY RESEARCH ACCOMPLISHMENTS

- Developed digital ELISA assays for PR (LOD=1.5 fM), ER-α (LOD=1fM), MCP-1 (LOD=7 fM), CYR61 (LOD=50fM), and LCN2 (LOD=1fM).
- Performed preliminary studies to measure PR and ER-α in mouse serum and obtained measurable quantities of each biomarker.
- Established a method to modify the current digital ELISA assay to apply to low cell protein measurements.
- Measured the PR content from as low as 100 cells and the PSA content from as low as 10 cells from the T-47D and LNCaP cell lines, respectively.
- Obtained serial and terminal bleeds from HIM model in mice with and without metastatic disease.
- Established 2 models of metastatic breast cancer in HIM model.
- Established techniques to sequence mtDNA from blood and FFPE tumor tissue
- Demonstrated that miR-720 levels are regulated by ADAM8
- Demonstrated that the ability of ADAM8 to promote a migratory and invasive phenotype is mediated, in part, by miR-720.
- Established a method to detect miRNAs in mouse serum
- Developed an eDAR platform with higher throughput, simpler fabrication, and better sensitivity for use in clinical studies to analyze cell biomarkers from breast cancer patients.
- Developed a method for storing whole blood for over 3 days so blood samples from mouse models and from patients can be shipped from Tufts or other hospital sites for analysis of cell biomarkers.
- Developed a technique based on sequential imaging and bleaching to study a large panel of biomarkers present on cancer cells.

REPORTABLE OUTCOMES

- Schubert, S. M., Baig, S., Walt, D. R. Single Molecule Assays for Early Breast Cancer Detection. Poster presented at: Tufts Cancer Center Symposium; 2013 June 25; North Grafton, MA.

- Schubert, S. M., Baig, S., Velasquez, E.F., Walt, D. R. Single Molecule Assays for Early Breast Cancer Detection. Poster presented at: Tufts Research Day on the Tufts Innovation Institute; 2013 September 20; Boston, MA.

- Sonia G. Das, Mathilde Romagnoli, Nora D. Mineva, Gail E. Sonenshein. MicroRNAs Downstream of ADAM8 as Therapeutic Targets and Non invasive Biomarkers for Triple Negative Breast Cancer. Poster session to be presented at AACR-NCI-EORTC Molecular Targets and Cancer Therapeutics Conference; October 19-23, 2013; Boston, MA

- M. Zhao, B. Wei, D.T. Chiu (2013) "Imaging multiple biomarkers in eDAR captured rare cells with sequential immunostaining and photobleaching" Method (in press)

- Y. Zhang, J. Yu, M.E. Gallina, W. Sun, Y. Rong, D.T. Chiu (2013) "Highly fluorescent fluorinated semiconducting polymer dots for cellular imaging and analysis" Chem. Comm. 49, 8256-8258.

- M. Zhao, W.C. Nelson, B. Wei, P.G. Schiro, B.M. Hakimi, E.S. Johnson, R.K. Perdue, G. Gyurkey, L.M. White, S. Whiting, D.T. Chiu (2013) "New generation of ensemble-decision aliquot ranking based on simplified microfluidic components for large-capacity trapping of circulating tumor cells" Anal. Chem. (submitted).

OVERALL SUMMARY AND CONCLUSION

In conclusion, great progress was made in the development of digital ELISA assays for the targeted breast cancer biomarkers. A total of five digital ELISA assays have now been successfully completed, most with LODs under 10 fM. Although some of these assays can still be optimized to gain more sensitivity, more focus will be placed on utilizing these assays for future mouse studies and on developing more digital ELISA assays.

Two single molecule assays, PR and ER- α were used to test serum samples obtained from mice with different cell line xenografts. Although protein was measured in both samples, the results were inconclusinve. Further experiments need to be performed for both biomarkers to determine the true values of both PR and ER- α in mouse serum.

Additionally, a novel method to determine protein content at the single molecule level in low numbers of cells was demonstrated. This assay was sensitive enough to measure the content of PSA down to five cells. Future work in the coming months will aim on improving this technique to gain single cell sensitivity.

REFERENCES

(1) Siegel, R.; Naishadham, D.; Jemal, A. *CA: A Cancer Journal for Clinicians* **2012**, *62*, 10.

(2) Rice, J. *Nature* **2012**, *485*, S55.

(3) Taplin, S.; Abraham, L.; Barlow, W. E.; Fenton, J. J.; Berns, E. A.; Carney, P. A.; Cutter, G. R.; Sickles, E. A.; Carl, D.; Elmore, J. G. *J Natl Cancer Inst* **2008**, *100*, 876.

(4) Jørgensen, K. J.; Gøtzsche, P. C. *BMJ* **2009**, *339*.

(5) Giljohann, D. A.; Mirkin, C. A. *Nature* **2009**, *462*, 462.

(6) Fu, X.-D.; Goglia, L.; Sanchez, A. M.; Flamini, M.; Giretti, M. S.; Tosi, V.; Genazzani, A. R.; Simoncini, T. *Endocr Relat Cancer* **2010**, *17*, 431.

(7) Rakha, E. A.; Reis-Filho, J. S.; Ellis, I. O. *Breast Cancer Res Treat* **2010**, *120*, 293.

(8) Negus, R. P.; Stamp, G. W.; Relf, M. G.; Burke, F.; Malik, S. T.; Bernasconi, S.; Allavena, P.; Sozzani, S.; Mantovani, A.; Balkwill, F. R. *The Journal of Clinical Investigation* **1995**, *95*, 2391.

(9) Yang, J.; Bielenberg, D. R.; Rodig, S. J.; Doiron, R.; Clifton, M. C.; Kung, A. L.; Strong, R. K.; Zurakowski, D.; Moses, M. A. *Proceedings of the National Academy of Sciences* **2009**, *106*, 3913.

(10) Menendez, J. A.; Mehmi, I.; Griggs, D. W.; Lupu, R. *Endocrine-Related Cancer* **2003**, *10*, 141.

(11) O'Kelly, J.; Chung, A.; Lemp, N.; Chumakova, K.; Yin, D.; Wang, H. J.; Said, J.; Gui, D.; Miller, C. W.; Karlan, B. Y.; Koeffler, H. P. *Int J Oncol* **2008**, *33*, 59.

(12) Wilson, D. H.; Hanlon, D. W.; Provuncher, G. K.; Chang, L.; Song, L.; Patel, P. P.; Ferrell, E. P.; Lepor, H.; Partin, A. W.; Chan, D. W.; Sokoll, L. J.; Cheli, C. D.; Thiel, R. P.; Fournier, D. R.; Duffy, D. C. *Clinical Chemistry* **2011**, *57*, 1712.

(13) J. Biol. Chem. 270: 24769-775, **1995**

(14) Mitochondrial DNA, 23: 106-111, **2012**